

Origin and emergent features of many-body dynamical localization

Ang Yang,^{1,*} Zekai Chen,^{2,*} Yanliang Guo,^{2,†} Manuele Landini,² Hanns-Christoph Nägerl,² and Lei Ying^{1,‡}

¹*School of Physics and Zhejiang Key Laboratory of Micro-nano Quantum Chips and Quantum Control, Zhejiang University, Hangzhou 310027, China*

²*Institut für Experimentalphysik und Zentrum für Quantenphysik, Universität Innsbruck, Technikerstraße 25, Innsbruck, 6020, Austria*

The question of whether interactions can break dynamical localization in quantum kicked rotor systems has been the subject of a long-standing debate. Here, we introduce an extended mapping from the kicked Lieb-Liniger model to an effective lattice model with long-range couplings and reveal two universal features: on-site pseudorandomness and rapidly decaying couplings in the center-of-mass momentum. For finite contact interactions, the long-range coupling between relative momenta obeys an algebraic decay behavior with a crossover of its decay exponent as the interaction increases. Similar behavior occurs in the Fock basis, underscoring the robustness and distinct many-body characteristics of dynamical localization. Analysis of the generalized fractal dimension and level-spacing ratio also supports these findings, highlighting the presence of near integrability and multifractality in different regions of parameter space. Our results offer an explanation for the occurrence of many-body dynamical localization, particularly in strongly correlated quantum gases, and are anticipated to generalize to systems of many particles.

Introduction.—Quantum coherence can give rise to captivating phenomena. For example, the quantum kicked rotor (QKR), as a driven single-particle system, exhibits dynamical localization (DL) [1–6]: non-resonant periodic driving paradoxically leads to suppressed energy absorption. Such an unexpected halt in energy growth in the quantum realm starkly contrasts our everyday experience, which tells us that driven systems generally thermalize to infinite temperature. DL for the QKR can be understood as Anderson localization (AL) in momentum space, characterized by a freezing of the momentum distribution in the course of its evolution [7, 8]. This behavior has been studied extensively in atomic experiments over the past three decades [9–16]. However, in reality, particles interact with each other. This raises a fundamental question: Can driven quantum systems avoid thermalization in the presence of inter-particle interactions? This challenge has spurred the development and investigation of various many-body QKR models, where particle-particle correlations are introduced through mechanisms such as periodic kicks [17–20] or static contact interactions [21–23]. These models predict a diverse range of behavior, including both DL and delocalized phases. Understanding the mechanism of localization sheds light on the role of many-body interactions in driven quantum systems.

The QKR model with contact interactions has received particular attention since it can be realized in cold-atom platforms. Predictions based on the mean-field approximation suggest that the system delocalizes at long times with a subdiffusive behavior of the energy [24–27], consistent with recent experimental observations [28, 29]. However, in one dimension, the mean-field approach runs into severe limitations [30, 31]. Beyond this approximation, numerical studies treating two interacting bosons have yielded contradictory results [23, 32]. In the Tonks-Girardeau (TG) regime, non-

perturbative techniques such as the Bose-Fermi mapping [33–38] predict that DL persists in the interacting many-body situation. This phenomenon has been called many-body dynamical localization (MBDL) [21, 22, 39]. It has been observed in recent experimental work [40]. The momentum distribution was shown to freeze over the entire range from weak to strong interactions despite the strong drive.

To date, most studies on MBDL have focused on obtaining the time evolution of the energy and the momentum distribution, starting from low-energy initial states [21, 22, 39]. However, the microscopic mechanism driving MBDL remains little understood. In this paper, we investigate MBDL in the Lieb-Liniger (LL) model [41–45] augmented by a kicking term [21]. Using the LL eigenstates as a basis, we establish an extended mapping from this quantum system to an effective lattice model beyond the well-known mapping from DL to AL. In the lattice model, we find that the off-diagonal matrix elements between LL eigenstates feature a combination of rapidly decaying lower bounds and algebraic tails, with the latter being the result of the interactions. The characteristic exponent for the algebraic decay exhibits a distinct dependence on the interaction strength. This provides crucial insight into the origin and characteristics of the MBDL phase. Our results indicate the existence of MBDL across the entire range of interaction strengths. This conclusion is further confirmed by an analysis in Fock basis and by inspecting the generalized fractal dimensions (GFD) and the energy-level-spacing statistics.

Model.—We consider the 1D kicked LL model, meant to describe N short-range interacting bosons of mass M_a constrained to a ring of circumference $L=2\pi$, subject to a pulsed sinusoidal potential [21, 22, 32], as illustrated in Fig. 1(a). With k numbering the kicks with period T , the Hamiltonian is written as the sum of the LL Hamiltonian and the kick Hamiltonian,

$$\hat{H}(t) = \hat{H}_1 + \sum_k \delta(t - kT) \hat{H}_K, \quad (1)$$

* These authors contributed equally to this work.

† yanliang.guo@uibk.ac.at

‡ leiying@zju.edu.cn

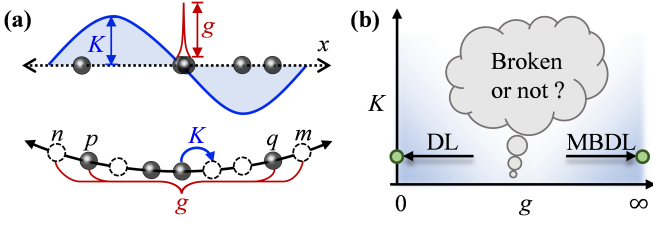


Figure 1. (a) Schematic of the kicked LL system in coordinate (upper) and momentum (lower) spaces, where blue and red curves denote the pulsed sinusoidal potential and the contact interactions, respectively. In momentum space, the kinetic energy component is represented by a quadratic potential defined over a momentum lattice. The periodic kicks introduce the couplings between adjacent momentum states. Boson-boson interactions result in momentum scattering, where the total momentum is conserved ($n + m = p + q$). (b) Schematic diagram of the kicked LL system as a function of the kick strength K and the interaction strength g . While DL and MBDL are respectively expected in the limiting scenarios of zero and infinite interactions (green circles), it is unclear for intermediate interactions.

with [21, 41]

$$\hat{H}_I = \sum_i \frac{\hat{p}_i^2}{2} + g \sum_{i < j} \delta(\hat{x}_i - \hat{x}_j) \text{ and } \hat{H}_K = K \sum_i \cos(\hat{x}_i). \quad (2)$$

The dimensionless parameters g and K denote the interaction strength and the kick strength, respectively. The various limits are well understood: For $K=0$ we recover the LL model. For $K \neq 0$, it is known that DL and MBDL occur in the two limits $g=0$ and $g=\infty$ [6, 21]. In both cases the problem can be mapped onto a single-particle problem. In the intermediate interaction regime, it is unclear whether localized phenomenon persists, as illustrated in Fig 1(b).

The momentum-space representation of the Hamiltonian in second quantization using the Fock basis $|\cdots n_m \cdots\rangle$ reads [46]

$$\begin{aligned} \hat{H}_I &= \frac{\hbar_{\text{eff}}^2}{2} \sum_{m=-\infty}^{\infty} m^2 \hat{b}_m^\dagger \hat{b}_m + \frac{g}{2L} \sum_{m,n,p,q} \hat{b}_m^\dagger \hat{b}_n^\dagger \hat{b}_p \hat{b}_q \delta_{m+n,p+q}, \\ \hat{H}_K &= \frac{K}{2} \sum_{m=-\infty}^{\infty} (\hat{b}_m^\dagger \hat{b}_{m+1} + \text{H.c.}), \end{aligned} \quad (3)$$

where \hat{b}_m^\dagger and \hat{b}_m are the bosonic creation and annihilation operators of momentum state m , obeying the commutation relations $[\hat{b}_m, \hat{b}_{m'}^\dagger] = \delta_{m,m'}$. Particle-number conservation requires $\sum_m \hat{b}_m^\dagger \hat{b}_m = N$. Here, $\hbar_{\text{eff}} = 4T\hbar k_V^2/M_a$ is an effective Planck constant [46], and we set $\hbar_{\text{eff}} = T = 1$. We perform exact diagonalization (ED) by introducing a bound on the maximally allowed single-particle momenta as $|m| \leq M$ [18, 47]. The dimension of the Hilbert space is determined by the binomial coefficient $\mathcal{N} = \binom{2M+N}{N}$. We further reduce the Hilbert space by only considering the parity sector of +1.

The one-period Floquet operator [48], $\hat{U} = \exp\{-iT\hat{H}_I/\hbar_{\text{eff}}\} \exp\{-i\hat{H}_K/\hbar_{\text{eff}}\}$, describes time evolution in the kicked LL model. Its eigenvalues are complex numbers

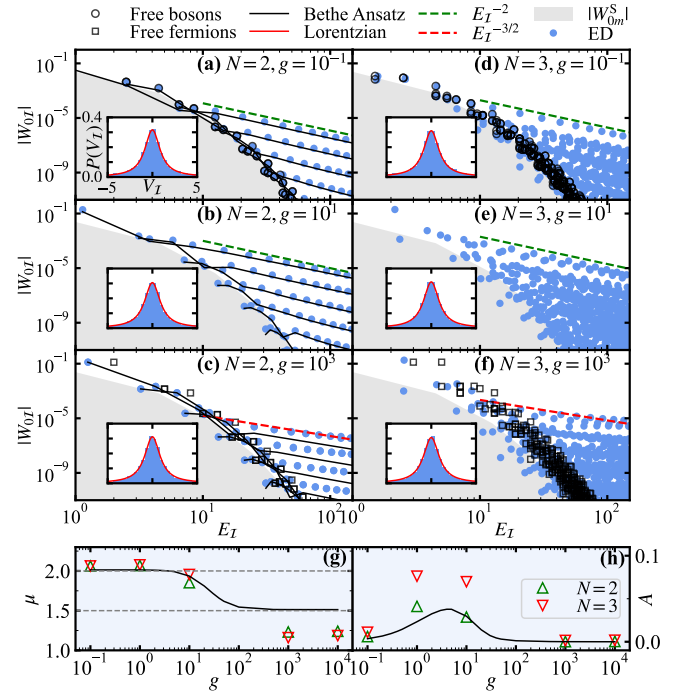


Figure 2. (a-c) The off-diagonal term $|W_{0I}|$ as a function of energy E_I for (a) $g = 10^{-1}$, (b) $g = 10^1$, and (c) $g = 10^3$ in log-log scale. The black lines stand for the Bethe-Ansatz results. The black circles and squares represent the off-diagonal term of the mapped free bosons and fermions, respectively. The red and green dashed lines denote algebraic decay as $E_I^{-3/2}$ and E_I^{-2} , respectively. Insets show the histograms of on-site term V_I , fitted by a Lorentzian distribution. The upper boundary of the gray shaded area denotes the off-diagonal term of the mapped single-particle $|W_{0m}^S|$. The momentum cut-off, the kick strength and the particle number are $M = 101$, $K = 0.5$ and $N = 2$, respectively. (d-f) show the same data as in (a-c) but for $N = 3$ and $M = 35$. Here, we set $\theta_a = 0$ and the multiple layers of tails are due to different center-of-mass momenta. (g, h) respectively show the decay exponent μ and amplitude A as a function of g , which are extracted from fitting the largest tail of $|W_{0I}|$ to a power-law function $AE_I^{-\mu}$.

with unit modulus $\hat{U} = \sum_{\alpha} \exp\{-i\theta_{\alpha}T/\hbar_{\text{eff}}\} |\phi_{\alpha}\rangle\langle\phi_{\alpha}|$, where quasienergies θ_{α} are chosen to be in $[-\pi\hbar_{\text{eff}}/T, \pi\hbar_{\text{eff}}/T]$.

Mapping to the lattice model.—It is well-known that the single-particle QKR can be mapped to an Anderson-like model [2, 8]. Here, we consider the many-body extension of the mapping. By introducing the eigenspectrum decomposition $\hat{H}_I = \sum_I E_I |I\rangle\langle I|$ and $\hat{H}_K = \sum_{\mathcal{K}} E_{\mathcal{K}} |\mathcal{K}\rangle\langle\mathcal{K}|$, the eigenvalue equation for the \hat{U} operator can be casted in the form [14, 46]

$$V_I \Pi_I + \sum_{I \neq I'} W_{II'} \Pi_{I'} = -W_{II} \Pi_I, \quad (4)$$

where $V_I = \tan[(E_I - \theta_{\alpha})T/2\hbar_{\text{eff}}]$, $W_{II'} = \sum_{\mathcal{K}} \tan(E_{\mathcal{K}}/2\hbar_{\text{eff}}) \langle I|\mathcal{K}\rangle\langle\mathcal{K}|I'\rangle$, and Π_I denotes the coefficient containing the information about the Floquet eigenstate. For $N = 1$ and $g = 0$, $\{|I\rangle\}$ and $\{|\mathcal{K}\rangle\}$ recover the single-particle momentum basis $\{|m\rangle\}$ and the coordinate basis $\{|x\rangle\}$. Then, we have the on-site term

$V_m^S = \tan[(\hbar_{\text{eff}}^2 m^2/2 - \theta_\alpha)T/2\hbar_{\text{eff}}]$ and the off-diagonal term $W_{mm'}^S = (1/L) \int_0^{2\pi} \tan(K \cos x/2\hbar_{\text{eff}}) \exp\{i(m-m')x\} dx$. In general, localization is expected since V_m are pseudorandom numbers drawn from a Lorentzian distribution and $W_{mm'}^S$ decays sufficiently fast [49].

For $N > 1$, the perturbation theory with weak interaction and the Bose-Fermi mapping with infinitely strong interaction yield [46]

$$W_{II'} \sim \begin{cases} W_{II'}^{\text{FB}} + gW_{II'}^{(1)} + O(g^2) & \text{for } g \rightarrow 0, \\ W_{II'}^{\text{FF}} & \text{for } g = \infty, \end{cases} \quad (5)$$

where superscripts ‘‘FB’’ and ‘‘FF’’ denote free bosons and free fermions, respectively. Since the LL eigenenergy E_I has a quadratic dependence on momentum for large momenta, V_I is always pseudorandom. Notice that the correction $gW_{II'}^{(1)}$ is proportional to g for $g \rightarrow 0$, but disappears for $g = \infty$. This implies a non-monotonic behavior at finite interactions.

By employing the Bethe-Ansatz technique for $N = 2$, we have the asymptotic behavior of the off-diagonal term as [23, 46]

$$|W_{QQ'}^{qq'}| \sim \begin{cases} \left| \frac{\mathcal{B}_{Q-Q'}^{(2)}(0)}{4\pi^2 A_g} \frac{1}{q^4} \right| & \text{for } 2qA_g \rightarrow \infty, q \gg q', \\ \left| \frac{\mathcal{B}_{Q-Q'}^{(2)}(0)q'A_g}{\pi^2} \frac{1}{q^3} \right| & \text{for } 2qA_g \rightarrow 0, q \gg q', \end{cases} \quad (6)$$

where $\mathcal{B}_{Q-Q'}^{(2)}(0) = \frac{K}{2\hbar_{\text{eff}}} \int_0^{2\pi} \frac{\cos(x_c) \exp[2i(Q-Q')x_c]}{\cos^2[K \cos(x_c)/\hbar_{\text{eff}}]} dx_c$ and $A_g = \hbar_{\text{eff}}^2/g$. $x_c = (x_1 + x_2)/2$ is the center-of-mass position. Q (q) and Q' (q') are the center-of-mass (relative) momentum of eigenstates I and I' , respectively. The kicks nontrivially couple to the hopping in the center of mass momentum $\mathcal{B}_{Q-Q'}^{(2)}(0)$, which decays exponentially with $|Q - Q'|$ and indicates DL in the center-of-mass momentum space. Generally, this is expected for any N since \hat{H}_I conserves the center-of-mass momentum [46]. In the relative momentum, there is indeed a non-monotonic behavior in the tail $q^{-\lambda}$ of the hopping $|W_{QQ'}^{qq'}|$ from $\lambda = 4$ to $\lambda = 3$ and the tail's amplitude is first proportional, then inversely proportional to g as g grows. Notably, Eq. (6) shows that the kicks only affect the amplitude of the power-law tail. The resulting power-law decay exponent exceeds the critical threshold of $3/2$, which is a sufficient condition for localization [50].

Next, we employ ED to obtain the LL eigenstates and compute the off-diagonal term $|W_{II'}|$ as a function of E_I , particularly for the case of $N = 3$. It approximately takes the form of $|W_{II'}| \sim |W_{QR}^{qr}|^{1/2}$ due to the quadratic LL spectrum for large momenta. In Fig. 2, starting from the ground state of the LL model, we calculate the off-diagonal term $|W_{0I}|$ for two and three particles at different interactions. For $N = 2$, the numerical results align quantitatively with the Bethe-Ansatz results. For $N=3$, the qualitative decay behavior as a function of energy is retained. Despite more quantum numbers being involved in the lattice model, we find that $|W_{0I}|$ still has a lower bound by free particles, as expected in Eq. (5). The lower bound is related to the hopping in the center-of-mass momentum, as $\mathcal{B}_{Q-Q'}^{(2)}(0)$ in Eq. (6). The on-site terms always obey

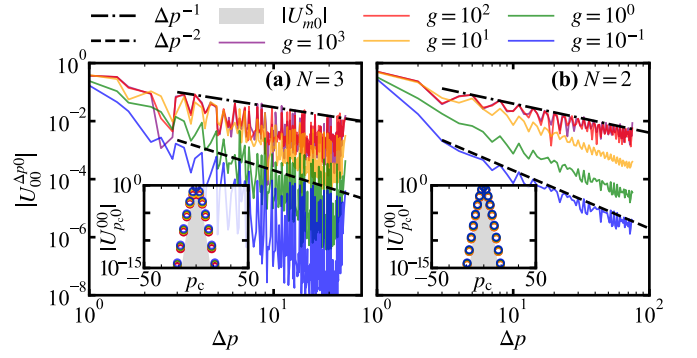


Figure 3. (a) The hopping amplitude as a function of the standard deviation Δp for the particle number $N = 3$ and different interactions g in log-log scale. The dashed line and dot-dashed line denote algebraic decay as Δp^{-2} and Δp^{-1} , respectively. Inset shows the hopping amplitudes as a function of the center-of-mass momentum p_c in semi-log scale. The upper boundary of the gray shaded area denotes the single-particle hopping $|U_{m0}^S|$. The cut-off and kick strength are $M = 30$ and $K = 1$, respectively. (b) The same data as in (a) but for $N = 2$ and $M = 75$.

Lorentzian distribution (insets). These features are retained from the single-particle case and the $N=2$ case. Remarkably, a clear algebraic tail of $|W_{0I}|$ emerges at high E_I , falling as $AE_I^{-\mu}$. For small g , the decay exponent μ remains constant, but its amplitude A depends on g . As g increases to 10^3 , μ undergoes a crossover from $\mu = 2$ to $\mu \approx 3/2$, similar to the crossover of λ in the $N = 2$ case. This behavior indicates that the characteristic decay exponent of the algebraic tails of $|W_{0I}|$ is dominated by interaction. Furthermore, we fit the decay exponent μ and amplitude A of the tail of $|W_{0I}|$ at large E_I , as shown in Figs. 2 (g) and (h). The Bethe-Ansatz results remarkably show a simultaneous crossover of μ and A with increasing g . Despite some deviations at large g which we ascribe to the finite momentum cutoff M , the numerical results for $N = 2, 3$ exhibit the same overall behavior. Therefore, we expect the above phenomena to hold for numerous interacting bosons. Similar behaviors are observed when computing the off-diagonal term from an excited state $I' \neq 0$ [46]. In the sense of large decay exponents, MBDL is expected across all values of g and the crossover of the algebraic tail indicates a distinct characterization of the high and low interaction regime.

Perspective from Fock basis.—It is noteworthy that the above mapping is done in LL eigenbasis. To connect to the experimentally accessible momentum distribution, we turn to study the Floquet operator in the Fock basis $\bigotimes_{i=1}^N |m_i\rangle$. For arbitrary N , we label a family of Fock states by $|\alpha\rangle \equiv |p_c, \Delta p\rangle$ with its center-of-mass momentum p_c and standard deviation Δp being

$$p_c = \sum_i m_i, \quad \Delta p = \left(N \sum_i m_i^2 - p_c^2 \right)^{1/2}. \quad (7)$$

Its kinetic energy is $E_m \propto p_c^2 + \Delta p^2$. We characterize the hopping amplitude in Fock basis as $|U_{p_c p_c'}^{\Delta p \Delta p'}| = \langle p_c, \Delta p | \hat{U} | p_c', \Delta p' \rangle$.

For $N = 1$, the hopping amplitude reduces to $|U_{m0}^S| = (-i)^m J_m(K/\hbar_{\text{eff}}) \exp\{-im^2/2\hbar_{\text{eff}}\}$ where $J_m(\dots)$ denotes m th-order Bessel function of the first kind. For $N > 1$, we consider the hopping amplitude starting from the zero-momentum state $|0, 0\rangle$. There are two cases for increased kinetic energy: (i) The growth of p_c while Δp remains fixed, leading to the acceleration of all bosons; (ii) The spreading of Δp while p_c remains fixed, facilitating long-range interactions of bosons in momentum space.

The hopping amplitudes of the above two cases are shown in Fig. 3 for three (a) and two (b) particles. As we expected, the hopping amplitude of the center-of-mass momentum growth $|U_{p_c 0}^{00}|$ follows a fast decay captured by the non-interacting result (insets), indicating DL. Notably, $|U_{p_c 0}^{00}|$ is only slightly affected by interactions. The hopping amplitude of Δp spreading also exhibits an algebraic tail, falling as $|U_{00}^{\Delta p 0}| \sim \Delta p^{-\nu}$. For a small g , say $g \leq 10^1$, the exponent of the tail remains constant as $\nu = 2$ and increasing g only affects the overall amplitude. Further increasing interaction up to $g = 10^2$, ν dramatically changes to 1 and stays constant hereafter. The crossover of ν corresponds to that of μ . For different fixed p_c , $|U_{p_c p_c}^{\Delta p 0}|$ holds similar behavior [46]. Similar crossover of the algebraic tail is found in the occupation spectrum of the one-particle density matrix [46]. The algebraic tail in $|U_{00}^{\Delta p 0}|$ also suggests that kicking a nonequilibrium state with various interactions can produce DL with different tails at steady state [46, 51].

Statistics of eigenstates.—Here we focus on the Floquet eigenspectrum and eigenstates for various kick strengths and interactions. We diagonalize \hat{U} , focus around the mid spectrum ($\theta_\alpha = 0$), typically extracting 500 eigenstates for various values of the cutoff M , ranging from 10 to 32. We first study the Floquet eigenstates based on the participation entropies (PE) S_β . Given an eigenstate $|\phi\rangle$ and a N -dimensional basis $\{|\alpha\rangle\}$, the PE are defined as [52–55]

$$S_\beta = \frac{1}{1-\beta} \ln \left(\sum_{\alpha=1}^N |\phi_\alpha|^{2\beta} \right), \quad |\phi\rangle = \sum_{\alpha=1}^N \phi_\alpha |\alpha\rangle. \quad (8)$$

Then one can define the GFD D_β as $D_\beta = \lim_{N \rightarrow \infty} S_\beta / \ln N$. If D_β nontrivially depends on β , the state is multifractal, whereas for constant D_β , the state is fractal [53]. For a fully delocalized state, $D_\beta = 1$, while $D_\beta = 0$ represents the scenario of Anderson localization. Values of $0 < D_\beta < 1$, indicate an extended but nonergodic state.

Fig. 4(a) shows the GFD D_3 as a function of the interaction strength g and the kick strength K , which is extracted from a linear fitting $\bar{S}_\beta = D_\beta \ln N + b_\beta$ [46]. Here, b_β is a subleading correction at finite dimension and negative b_β can be related to a nonergodic volume $\Lambda = e^{-b_\beta}$ [52]. \bar{S}_β denotes the averaged S_β over 500 eigenstates. One can notice three regimes: (I) $D_3 \geq 0$; (II) $0.4 \lesssim D_3 < 1$; (III) $D_3 \sim 0.4$. We focus on the kick strength $K = 1$, as shown in Fig. 4(c). When g is small, $D_3 \geq 0$, thus the Floquet eigenstate is highly localized at regime I. Notably, increasing g from the weakly interacting regime ($g \sim 10^{-2}, \gamma \ll 1$) up to the strongly correlated regime ($g \sim 0.48, \gamma = 1$) does not correspond to a remarkable increase in D_3 , contrary to delocalization predicted by

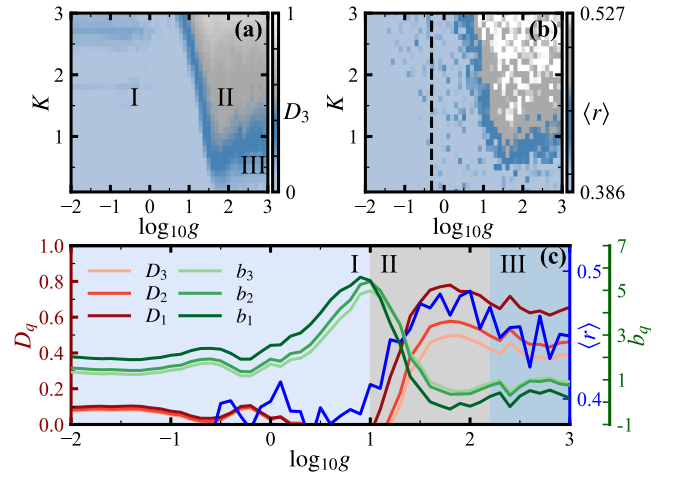


Figure 4. (a) The GFD D_3 as a function of the interaction strength g and the kick strength K . (b) The averaged energy-level-spacing ratio $\langle r \rangle$ as a function of g and K for $M = 32$. The black dashed line denotes where the LL parameter is $\gamma = 1$. The area at larger K and g represents numerical inaccurate regime due to finite truncation. (c) Different D_β , b_β , and $\langle r \rangle$ as a function of g for $K = 1.0$. The shaded areas denote different regimes. The number of bosons is $N = 3$.

the mean-field approximation. Further increasing g in regime II, D_3 exhibits a dramatic increase, while the fitted intercept b_3 drops sharply and then levels off near zero. In this regime, the Floquet eigenstates are highly extended ($0.4 \lesssim D_3 < 1$) but remain nonergodic. As g approaches regime III, D_3 decreases. This reduction is attributed to the fermionization of the bosons as g approaches infinity, at which point the system behaves like a TG gas [33–36]. Similar behavior is found for $\beta = 1, 2$. Therefore, the GFD of the kicked LL model exhibits a non-monotonic change with increasing interaction strength, diagnosing the MBDL phase and its distinct signatures. Such a behavior aligns with the crossover of the tail of the hopping matrix both in LL and Fock basis, and is also consistent with the recently predicted non-monotonic change in localized interaction energy [32]. Here, we notice that $D_3 \neq D_2 \neq D_1$, thus the MBDL phase is multifractal. At larger kick strengths, similar qualitative behavior is expected. The diagram in Fig. 4(a) agrees with the qualitative picture in Fig. 1(b), except for the notable finding that the eigenstates remain nonergodic in regime II.

In Figs. 4(b) and (c), we plot the level-spacing ratio by averaging $r_\alpha = \min(\delta_{\alpha+1}, \delta_\alpha) / \max(\delta_{\alpha+1}, \delta_\alpha)$ with $\delta_\alpha = \theta_{\alpha+1} - \theta_\alpha$. For a Floquet system, the averaged ratio $\langle r \rangle$ allows one to distinguish whether its level-spacing distribution belongs to the Poisson type or the circular orthogonal ensemble (COE) [49]. The former type corresponds to an integrable system with $\langle r \rangle \approx 0.386$, whereas the latter one means that the system is ergodic with $\langle r \rangle \approx 0.5269$ [56, 57]. We find high similarities between the diagram obtained by D_3 and $\langle r \rangle$. Regime I corresponds to where $\langle r \rangle$ approaches the integrable value of 0.386, suggesting that the MBDL is near-integrable at regime I. In regime II, $\langle r \rangle$ increases greatly but does not reach the ergodic value, consistent with the extended Floquet states. Then, due

to fermionization, $\langle r \rangle$ decreases in regime III and displays again the nearly integrable behavior. For a given kick strength, these results indicate that the kicked LL model remains nonergodic and the MBDL phase is dominated by different features at different interactions.

Discussions.—In summary, we have investigated the microscopic origin of the MBDL phase in the kicked LL model. Given a fixed kick strength, we find that arbitrary contact interaction strengths do not disrupt dynamical localization. However, finite interactions introduce an algebraic tail to the localization properties, observed both in the LL eigenbasis and in the Fock basis. The exponent and amplitude of this algebraic tail exhibit a nontrivial dependence on the interaction strength, reflecting the characteristic features of the MBDL phase. Further analysis of the many-body eigenstates suggests that MBDL possesses multifractal properties and that finite interactions render the system non-integrable. Our study provides an explanation for the longstanding question of MBDL's existence at finite interaction strengths and is anticipated to be valid for systems with many particles.

At intermediate interaction strengths, the Floquet eigenstates become extended and the level statistics deviate from the integrable regime. This indicates the presence of quantum chaos. Crucial open questions remain: How does quantum

chaos arise in the kicked LL model at finite interaction strengths? Is there a critical kick strength beyond which the MBDL is absent? Despite our explanation for the MBDL, future theoretical and experimental investigations are urgently needed. Moreover, the ubiquitous algebraic tail of the momentum distribution, particularly at weak interactions, exhibits a phenomenological resemblance to that observed in quantum turbulence [58, 59]. This similarity warrants further investigation to substantiate a potential link between these phenomena.

Acknowledgment.—We thank Prof. Chushun Tian for many helpful suggestions. We also thank Prof. Marcos Rigol for discussions. This work was supported by the National Key R&D Program of China under grant No. 2022YFA1404203 and the National Natural Science Foundation of China under grant No. 12375021. The Innsbruck team acknowledges funding by a Wittgenstein prize grant with the Austrian Science Fund (FWF) project number Z336-N36, by the European Research Council (ERC) with project number 789017, by an FFG infrastructure grant with project number FO999896041, and by the FWF's COE 1 and quantA. Y.G. is supported by the FWF with project number 10.55776/COE1.

Note.—As we finalized our paper, we found that H. Olsen *et al.* [60] independently posted a preprint on the same topic at the same time.

-
- [1] G. Casati, B. V. Chirikov, F. M. Izraelev, and J. Ford, Stochastic behavior of a quantum pendulum under a periodic perturbation, in *Stochastic Behavior in Classical and Quantum Hamiltonian Systems*, edited by G. Casati and J. Ford (Springer Berlin Heidelberg, Berlin, Heidelberg, 1979) pp. 334–352.
- [2] S. Fishman, D. R. Grempel, and R. E. Prange, Chaos, quantum recurrences, and anderson localization, *Phys. Rev. Lett.* **49**, 509 (1982).
- [3] B. V. Chirikov and D. L. Shepelyanskii, Localization of dynamical chaos in quantum systems, *Radiophysics and Quantum Electronics* **29** (1986).
- [4] A. Altland, Diagrammatic approach to anderson localization in the quantum kicked rotor, *Phys. Rev. Lett.* **71**, 69 (1993).
- [5] A. Altland and M. R. Zirnbauer, Field theory of the quantum kicked rotor, *Phys. Rev. Lett.* **77**, 4536 (1996).
- [6] M. Santhanam, S. Paul, and J. B. Kannan, Quantum kicked rotor and its variants: Chaos, localization and beyond, *Physics Reports* **956**, 1 (2022).
- [7] P. W. Anderson, Absence of diffusion in certain random lattices, *Phys. Rev.* **109**, 1492 (1958).
- [8] D. R. Grempel, R. E. Prange, and S. Fishman, Quantum dynamics of a nonintegrable system, *Phys. Rev. A* **29**, 1639 (1984).
- [9] F. L. Moore, J. C. Robinson, C. Bharucha, P. E. Williams, and M. G. Raizen, Observation of dynamical localization in atomic momentum transfer: A new testing ground for quantum chaos, *Phys. Rev. Lett.* **73**, 2974 (1994).
- [10] F. L. Moore, J. C. Robinson, C. F. Bharucha, B. Sundaram, and M. G. Raizen, Atom optics realization of the quantum δ -kicked rotor, *Phys. Rev. Lett.* **75**, 4598 (1995).
- [11] B. G. Klappauf, W. H. Oskay, D. A. Steck, and M. G. Raizen, Observation of noise and dissipation effects on dynamical localization, *Phys. Rev. Lett.* **81**, 1203 (1998).
- [12] H. Ammann, R. Gray, I. Shvarchuck, and N. Christensen, Quantum delta-kicked rotor: Experimental observation of decoherence, *Phys. Rev. Lett.* **80**, 4111 (1998).
- [13] J. Chabé, G. Lemarié, B. Grémaud, D. Delande, P. Szriftgiser, and J. C. Garreau, Experimental observation of the anderson metal-insulator transition with atomic matter waves, *Phys. Rev. Lett.* **101**, 255702 (2008).
- [14] G. Lemarié, J. Chabé, P. Szriftgiser, J. C. Garreau, B. Grémaud, and D. Delande, Observation of the anderson metal-insulator transition with atomic matter waves: Theory and experiment, *Phys. Rev. A* **80**, 043626 (2009).
- [15] I. Manai, J.-F. m. c. Clément, R. Chicireanu, C. Hainaut, J. C. Garreau, P. Szriftgiser, and D. Delande, Experimental observation of two-dimensional anderson localization with the atomic kicked rotor, *Phys. Rev. Lett.* **115**, 240603 (2015).
- [16] M. B. d'Arcy, R. M. Godun, M. K. Oberthaler, D. Cassettari, and G. S. Summy, Quantum enhancement of momentum diffusion in the delta-kicked rotor, *Phys. Rev. Lett.* **87**, 074102 (2001).
- [17] S. Notarnicola, F. Iemini, D. Rossini, R. Fazio, A. Silva, and A. Russomanno, From localization to anomalous diffusion in the dynamics of coupled kicked rotors, *Phys. Rev. E* **97**, 022202 (2018).
- [18] A. Russomanno, M. Fava, and R. Fazio, Chaos and subdiffusion in infinite-range coupled quantum kicked rotors, *Phys. Rev. B* **103**, 224301 (2021).
- [19] E. B. Rozenbaum and V. Galitski, Dynamical localization of coupled relativistic kicked rotors, *Phys. Rev. B* **95**, 064303 (2017).
- [20] A. C. Keser, S. Ganeshan, G. Refael, and V. Galitski, Dynamical many-body localization in an integrable model, *Phys. Rev. B* **94**, 085120 (2016).

- [21] C. Rylands, E. B. Rozenbaum, V. Galitski, and R. Konik, Many-body dynamical localization in a kicked lieb-liniger gas, *Phys. Rev. Lett.* **124**, 155302 (2020).
- [22] V. Vuatelet and A. Rançon, Effective thermalization of a many-body dynamically localized bose gas, *Phys. Rev. A* **104**, 043302 (2021).
- [23] P. Qin, A. Andreanov, H. C. Park, and S. Flach, Interacting ultracold atomic kicked rotors: loss of dynamical localization, *Scientific Reports* **7**, 41139 (2017).
- [24] S. Lellouch, A. Rançon, S. De Bièvre, D. Delande, and J. C. Garreau, Dynamics of the mean-field-interacting quantum kicked rotor, *Phys. Rev. A* **101**, 043624 (2020).
- [25] G. Gligorić, J. D. Bodyfelt, and S. Flach, Interactions destroy dynamical localization with strong and weak chaos, *Europhysics Letters* **96**, 30004 (2011).
- [26] D. L. Shepelyansky, Delocalization of quantum chaos by weak nonlinearity, *Phys. Rev. Lett.* **70**, 1787 (1993).
- [27] A. S. Pikovsky and D. L. Shepelyansky, Destruction of anderson localization by a weak nonlinearity, *Phys. Rev. Lett.* **100**, 094101 (2008).
- [28] J. See Toh, K. McCormick, X. Tang, S. Ying, X.-W. Luo, C. Zhang, and S. Gupta, Many-body dynamical delocalization in a kicked one-dimensional ultracold gas, *Nature Physics* **18**, 1297 (2022).
- [29] A. Cao, R. Sajjad, H. Mas, E. Q. Simmons, J. L. Tanlimco, E. Nolasco-Martinez, T. Shimasaki, H. E. Kondakci, V. Galitski, and D. M. Weld, Interaction-driven breakdown of dynamical localization in a kicked quantum gas, *Nature Physics* **18**, 1302 (2022).
- [30] T. Giamarchi, *Quantum Physics in One Dimension* (Oxford University Press, 2003).
- [31] A. O. Gogolin, A. A. Nersisyan, and A. M. Tsvelik, *Bosonization and Strongly Correlated Systems* (Cambridge University Press, 2004).
- [32] R. Chicireanu and A. Rançon, Dynamical localization of interacting bosons in the few-body limit, *Phys. Rev. A* **103**, 043314 (2021).
- [33] M. Girardeau, Relationship between systems of impenetrable bosons and fermions in one dimension, *Journal of Mathematical Physics* **1**, 516 (1960).
- [34] H. Buljan, R. Pezer, and T. Gasenzer, Fermi-Bose transformation for the time-dependent Lieb-Liniger gas, *Phys. Rev. Lett.* **100**, 080406 (2008).
- [35] M. Rigol and A. Muramatsu, Ground-state properties of hardcore bosons confined on one-dimensional optical lattices, *Phys. Rev. A* **72**, 013604 (2005).
- [36] V. I. Yukalov and M. D. Girardeau, Fermi-bose mapping for one-dimensional bose gases, *Laser Physics Letters* **2**, 375 (2005).
- [37] B. Paredes, A. Widera, V. Murg, O. Mandel, S. Fölling, I. Cirac, G. V. Shlyapnikov, T. W. Hänsch, and I. Bloch, Tonks-girardeau gas of ultracold atoms in an optical lattice, *Nature* **429**, 277 (2004).
- [38] J. M. Wilson, N. Malvania, Y. Le, Y. Zhang, M. Rigol, and D. S. Weiss, Observation of dynamical fermionization, *Science* **367**, 1461 (2020).
- [39] V. Vuatelet and A. Rançon, Dynamical many-body delocalization transition of a Tonks gas in a quasi-periodic driving potential, *Quantum* **7**, 917 (2023).
- [40] Y. Guo, S. Dhar, A. Yang, Z. Chen, H. Yao, M. Horvath, L. Ying, M. Landini, and H.-C. Nägerl, Observation of many-body dynamical localization, [arXiv:2312.13880](https://arxiv.org/abs/2312.13880) (2023).
- [41] E. H. Lieb and W. Liniger, Exact analysis of an interacting bose gas. i. the general solution and the ground state, *Phys. Rev.* **130**, 1605 (1963).
- [42] E. H. Lieb, Exact analysis of an interacting bose gas. ii. the excitation spectrum, *Phys. Rev.* **130**, 1616 (1963).
- [43] M. Olshanii, Atomic scattering in the presence of an external confinement and a gas of impenetrable bosons, *Phys. Rev. Lett.* **81**, 938 (1998).
- [44] V. Dunjko, V. Lorent, and M. Olshanii, Bosons in cigar-shaped traps: Thomas-fermi regime, tonks-girardeau regime, and in between, *Phys. Rev. Lett.* **86**, 5413 (2001).
- [45] M. A. Cazalilla, R. Citro, T. Giamarchi, E. Orignac, and M. Rigol, One dimensional bosons: From condensed matter systems to ultracold gases, *Rev. Mod. Phys.* **83**, 1405 (2011).
- [46] See supplementary materials.
- [47] P. Weinberg and M. Bukov, QuSpin: a Python package for dynamics and exact diagonalisation of quantum many body systems. Part II: bosons, fermions and higher spins, *SciPost Phys.* **7**, 020 (2019).
- [48] P. Ponte, Z. Papić, F. m. c. Huvneers, and D. A. Abanin, Many-body localization in periodically driven systems, *Phys. Rev. Lett.* **114**, 140401 (2015).
- [49] F. Haake, *Quantum signatures of chaos* (Springer, 1991).
- [50] F. A. B. F. de Moura, A. V. Malyshev, M. L. Lyra, V. A. Malyshev, and F. Domínguez-Adame, Localization properties of a one-dimensional tight-binding model with nonrandom long-range intersite interactions, *Phys. Rev. B* **71**, 174203 (2005).
- [51] J. C. Zill, T. M. Wright, K. V. Kheruntsyan, T. Gasenzer, and M. J. Davis, Relaxation dynamics of the lieb-liniger gas following an interaction quench: A coordinate bethe-ansatz analysis, *Phys. Rev. A* **91**, 023611 (2015).
- [52] N. Macé, F. Alet, and N. Laflorencie, Multifractal scalings across the many-body localization transition, *Phys. Rev. Lett.* **123**, 180601 (2019).
- [53] A. Sarkar, A. Dheer, and S. Kumar, Multifractal dimensions for orthogonal-to-unitary crossover ensemble, [arXiv:2310.03526](https://arxiv.org/abs/2310.03526) (2023).
- [54] I. García-Mata, O. Giraud, B. Georgeot, J. Martin, R. Dubertrand, and G. Lemarié, Scaling theory of the anderson transition in random graphs: Ergodicity and universality, *Phys. Rev. Lett.* **118**, 166801 (2017).
- [55] Y. Wang, C. Cheng, X.-J. Liu, and D. Yu, Many-body critical phase: Extended and nonthermal, *Phys. Rev. Lett.* **126**, 080602 (2021).
- [56] L. D'Alessio and M. Rigol, Long-time behavior of isolated periodically driven interacting lattice systems, *Phys. Rev. X* **4**, 041048 (2014).
- [57] A. Lazarides, A. Das, and R. Moessner, Equilibrium states of generic quantum systems subject to periodic driving, *Phys. Rev. E* **90**, 012110 (2014).
- [58] V. Zakharov, P. Guyenne, A. Pushkarev, and F. Dias, Wave turbulence in one-dimensional models, *Physica D: Nonlinear Phenomena* **152-153**, 573 (2001).
- [59] V. Zakharov, F. Dias, and A. Pushkarev, One-dimensional wave turbulence, *Physics Reports* **398**, 1 (2004).
- [60] H. Olsen, P. Devillard, G. Aupetit-Diallo, P. Vignolo, and M. Albert, Interaction induced anderson transition in a kicked one dimensional bose gas, [arXiv:2503.02565](https://arxiv.org/abs/2503.02565) (2025).
- [61] S. Bera, H. Schomerus, F. Heidrich-Meisner, and J. H. Bardarson, Many-body localization characterized from a one-particle perspective, *Phys. Rev. Lett.* **115**, 046603 (2015).
- [62] D. A. Abanin, E. Altman, I. Bloch, and M. Serbyn, Colloquium: Many-body localization, thermalization, and entanglement, *Rev. Mod. Phys.* **91**, 021001 (2019).

Supplementary Materials for “Origin and emergent features of many-body dynamical localization”

S1. THE DIMENSIONLESS LIEB-LINIGER PARAMETER

It is known that the strength of the interaction for 1D Lieb-Liniger system can be captured by [38]

$$\gamma = \frac{M_a g_{1D}}{n_{1D} \hbar^2}, \quad (S1)$$

where g_{1D} is the strength of the effective one-dimensional contact interaction and n_{1D} is the particle density. Following the dimensionless transformation in Ref. [40], we have

$$g_{1D} = \frac{M_a g}{8k_L^3 T^2}, \quad \hbar_{\text{eff}} = \frac{4T \hbar k_L^2}{M_a}, \quad n_{1D} = \frac{2k_L N}{L}. \quad (S2)$$

Then, the dimensionless Lieb-Liniger parameter is given by

$$\gamma = \frac{gL}{N \hbar_{\text{eff}}^2}, \quad (S3)$$

which allows us to determine whether the system is in the strong interaction limit ($\gamma \gg 1$, degenerate solved) or the weak interaction limit ($\gamma \ll 1$, degenerate). Particularly, in our simulations for $N = 3$, the system reaches the strongly correlated regime at $g \sim 0.48$ ($\gamma = 1$), where the theory under mean-field approximate becomes invalid.

S2. DERIVATION OF HAMILTONIAN IN THE BOSONIC REPRESENTATION

In the context of the second quantization, the general form of a two-body interacting Hamiltonian reads

$$\hat{H}(t) = \int \hat{\Psi}^\dagger(x) \hat{h}(x, t) \hat{\Psi}(x) dx + \frac{1}{2} \iint \hat{\Psi}^\dagger(x) \hat{\Psi}^\dagger(x') U(x, x') \hat{\Psi}(x) \hat{\Psi}(x') dx dx', \quad (S4)$$

where $\hat{h}(x)$ and $U(x, x')$ represent the one-body Hamiltonian and the two-body interacting potential, respectively. $\hat{\Psi}(x)$ is the field operator. For the many-body quantum kicked rotor model, we have

$$\hat{h}(x, t) = -\frac{\hbar_{\text{eff}}^2}{2} \frac{\partial^2}{\partial x^2} + K \cos(x) \sum_n \delta(t - n), \quad U(x, x') = g \delta(x - x'). \quad (S5)$$

By expanding the field operator $\hat{\Psi}(x)$ in the complete single-particle momentum basis $\psi_m(x) = (1/\sqrt{L})e^{-imx}$, we have

$$\hat{\Psi}(x) = \sum_{m=-\infty}^{\infty} \psi_m(x) \hat{b}_m, \quad \hat{\Psi}^\dagger(x) = \sum_{m=-\infty}^{\infty} \psi_m^*(x) \hat{b}_m^\dagger. \quad (S6)$$

Intuitively, the total Hilbert space is expanded by the tensor products of all possible single-particle states $\bigotimes_{i=1}^N |m_i\rangle$. Considering the nature of bosons, the system is fully symmetric under permutations. Then the basis of Hilbert space is restricted as

$$|n_{-\infty} \cdots n_m \cdots n_{+\infty}\rangle = \sqrt{\frac{\prod_m n_m!}{N!}} \sum_P \hat{P} |m_1 m_2 \cdots m_N\rangle, \quad (S7)$$

where $\hat{n}_m = \hat{b}_m^\dagger \hat{b}_m$ is the particle number occupying on state m and \hat{P} denotes the permutation operator. In this representation, we have the following rules:

$$\begin{aligned} \hat{b}_m^\dagger |n_{-\infty} \cdots n_m \cdots n_{+\infty}\rangle &= \sqrt{n_m + 1} |n_{-\infty} \cdots n_m + 1 \cdots n_{+\infty}\rangle, \\ \hat{b}_m |n_{-\infty} \cdots n_m \cdots n_{+\infty}\rangle &= \sqrt{n_m} |n_{-\infty} \cdots n_m - 1 \cdots n_{+\infty}\rangle. \end{aligned} \quad (S8)$$

Substituting Eqs. (S5) and (S6) into Eq. (S4), we have

$$\begin{aligned} \hat{H}(t) = & \int \sum_{m,m'} \frac{\hbar_{\text{eff}}^2 m^2}{2} \psi_m^*(x) \psi_{m'}(x) \hat{b}_m^\dagger \hat{b}_{m'} dx + \int \sum_{m,m'} \frac{K}{2} [\psi_{m+1}^*(x) \psi_{m'}(x) + \psi_m^*(x) \psi_{m'+1}(x)] \hat{b}_m^\dagger \hat{b}_{m'} dx \sum_n \delta(t-n) \\ & + \int \sum_{m,n,p,q} \frac{g}{2L} \psi_{m+n}^*(x) \psi_{p+q}(x) \hat{b}_m^\dagger \hat{b}_n^\dagger \hat{b}_p \hat{b}_q dx. \end{aligned} \quad (\text{S9})$$

Utilizing the orthogonality and completeness of the basis that $\int \psi_m^*(x) \psi_{m'}(x) dx = \delta_{m,m'}$, the total Hamiltonian can be expressed as

$$\hat{H}(t) = \sum_{m=-\infty}^{\infty} \frac{\hbar_{\text{eff}}^2 m^2}{2} \hat{b}_m^\dagger \hat{b}_m + \frac{g}{2L} \sum_{m,n,p,q} \hat{b}_m^\dagger \hat{b}_n^\dagger \hat{b}_p \hat{b}_q \delta_{m+n,p+q} + \frac{K}{2} \left(\sum_{m=-\infty}^{\infty} \hat{b}_m^\dagger \hat{b}_{m+1} + \text{h.c.} \right) \sum_n \delta(t-n). \quad (\text{S10})$$

S3. DETAILS OF THE LATTICE MAPPING AND QUALITATIVE ANALYSIS

A. General mapping to the lattice model

According to Floquet's theorem, the Floquet eigenstates read

$$\hat{U}|\phi_\alpha\rangle = e^{-i\frac{\theta_\alpha T}{\hbar_{\text{eff}}}} |\phi_\alpha\rangle, \quad (\text{S11})$$

where $0 < \theta_\alpha \leq 2\pi\hbar_{\text{eff}}$ is the corresponding quasienergy. Firstly, we introduce the following expression

$$e^{-i\frac{\hat{H}_K}{\hbar_{\text{eff}}}} = \sum_{\mathcal{K}} \frac{1 - i \tan\left(\frac{E_{\mathcal{K}}}{2\hbar_{\text{eff}}}\right)}{1 + i \tan\left(\frac{E_{\mathcal{K}}}{2\hbar_{\text{eff}}}\right)} |\mathcal{K}\rangle \langle \mathcal{K}| \quad (\text{S12})$$

with spectral decomposition $\hat{H}_K = \sum_{\mathcal{K}} E_{\mathcal{K}} |\mathcal{K}\rangle \langle \mathcal{K}|$. Similarly, the static part can be written as

$$e^{-i\frac{T}{\hbar_{\text{eff}}}(\hat{H}_I - \theta_\alpha)} = \sum_I \frac{1 - i \tan\left(\frac{E_I - \theta_\alpha}{2\hbar_{\text{eff}}}\right)}{1 + i \tan\left(\frac{E_I - \theta_\alpha}{2\hbar_{\text{eff}}}\right)} |I\rangle \langle I|, \quad (\text{S13})$$

where $|I\rangle$ and E_I denote the eigenstate and eigenenergy of \hat{H}_I , respectively. Then, one can make the following expansion in the interacting eigenbasis $\{|I\rangle\}$ [14]

$$\sum_{\mathcal{K}} \frac{1}{1 + i \tan\left(\frac{E_{\mathcal{K}}}{2\hbar_{\text{eff}}}\right)} |\mathcal{K}\rangle \langle \mathcal{K}| \phi_\alpha = \sum_I \Pi_I |I\rangle. \quad (\text{S14})$$

Substituting Eqs. (S12), (S13), and (S14) into Eq. (S11), we have the discrete form of the Schrödinger equation as

$$V_I \Pi_I + \sum_{I \neq I'} W_{II'} \Pi_{I'} = -W_{II} \Pi_I, \quad (\text{S15})$$

where $V_I = \tan[(E_I - \theta_\alpha)T/2\hbar_{\text{eff}}]$ and $W_{II'} = \sum_{\mathcal{K}} \tan(E_{\mathcal{K}}/2\hbar_{\text{eff}}) \langle I|\mathcal{K}\rangle \langle \mathcal{K}|I'\rangle$ are the on-site potential and off-diagonal hopping, respectively.

B. The perturbative case

For $N > 1$ with $g \neq 0$, we divide \hat{H}_I into three parts in the Fock basis: the free part \hat{H}_0 , the g -dependent diagonal part \hat{H}_{ID} and off-diagonal part \hat{H}_{IOD} . They are respectively given by

$$\hat{H}_I = \hat{H}_0 + g\hat{H}_{\text{ID}} + g\hat{H}_{\text{IOD}}, \quad (\text{S16})$$

where

$$\hat{H}_0 = \frac{1}{2} \sum_{m=-\infty}^{\infty} \hbar_{\text{eff}}^2 m^2 \hat{n}_m, \quad \hat{H}_{\text{ID}} = \frac{1}{2L} \sum_{p,q} \hat{n}_p \hat{n}_q, \quad \hat{H}_{\text{IOD}} = \frac{1}{2L} \sum_{m \neq p, m \neq q} \hat{b}_m^\dagger \hat{b}_n^\dagger \hat{b}_p \hat{b}_q \delta_{m+n,p+q}. \quad (\text{S17})$$

There are two scenarios:

(i) If \hat{H}_{IOD} is ignored, then the on-site term V_I becomes g -dependent nonlinear disorder while $W_{II'}$ still decays rapidly. In such a nonlinear lattice model, localization is expected.

(ii) Considering small g and non-degenerate case, one can apply the perturbation theory to expand the eigenenergy as $E_I = E_I^{(0)} + gE_I^{(1)} + g^2E_I^{(2)}$ and eigenfunction as $|I\rangle = |I^{(0)}\rangle + g|I^{(1)}\rangle$. Here, $|I^{(0)}\rangle$ is the eigenstate of \hat{H}_0 . In this scenario, we have

$$E_I^{(1)} = \langle I^{(0)} | \hat{H}_{\text{IOD}} | I^{(0)} \rangle, \quad E_I^{(2)} = \sum_{I' \neq I} \frac{|\langle I'^{(0)} | \hat{H}_{\text{IOD}} | I^{(0)} \rangle|^2}{E_I^{(0)} - E_{I'}^{(0)}}, \quad |I^{(1)}\rangle = \sum_{I' \neq I} \frac{\langle I'^{(0)} | \hat{H}_{\text{IOD}} | I^{(0)} \rangle}{E_I^{(0)} - E_{I'}^{(0)}} |I'^{(0)}\rangle. \quad (\text{S18})$$

Substituting the equations above into Eq. (S15), we have the diagonal term as

$$V_I = \tan \left(\frac{E_I^{(0)} + gE_I^{(1)} + g^2E_I^{(2)} - \theta_\alpha}{2\hbar_{\text{eff}}} T \right), \quad (\text{S19})$$

and the off-diagonal term as

$$W_{II'} = W_{II'}^{(0)} + g \sum_{I'' \neq I'} \frac{\langle I''^{(0)} | \hat{H}_{\text{IOD}} | I'^{(0)} \rangle}{E_{I'}^{(0)} - E_{I''}^{(0)}} W_{II''}^{(0)} + g \sum_{I'' \neq I} \frac{\langle I^{(0)} | \hat{H}_{\text{IOD}} | I''^{(0)} \rangle}{E_I^{(0)} - E_{I''}^{(0)}} W_{I''I'}^{(0)} + O(g^2), \quad (\text{S20})$$

where the unperturbed hopping is $W_{II'}^{(0)} = \sum_{\mathcal{K}} \tan(E_{\mathcal{K}}/2\hbar_{\text{eff}}) \langle I^{(0)} | \mathcal{K} \rangle \langle \mathcal{K} | I'^{(0)} \rangle$. Thus, the off-diagonal hopping consists of the hopping of free bosons (FB) and g -dependent corrections.

C. The Tonks-Girardeau limit

Next, we consider the non-perturbative case with $g \rightarrow \infty$. In this case, the strong local repulsion leads to the situation that different bosons cannot simultaneously occupy the same position x , i.e., the hard-core bosons or Tonks-Girardeau (TG) gas. Utilizing the technique of the Bose-Fermi mapping, the eigenstate of the TG gas straightforwardly takes the form of a Slater determinant and the TG gas have similar spectrum as free fermions. Thus, we have [21, 45]

$$|I\rangle = \int dx^N \mathcal{A} \det [\psi_{m_k}^I(x_k)] \prod_{i=1}^N \hat{b}_{x_i}^\dagger |0\rangle, \quad E_I = \frac{1}{2} \sum_{k=1}^N \hbar_{\text{eff}}^2 m_k^2, \quad (\text{S21})$$

where $\mathcal{A} = \prod_{1 \leq i < j \leq N} \text{sgn}(x_i - x_j)$ is the antisymmetrizer which guarantees the permutation symmetry of the bosonic wave function and $\psi_{m_k}^I(x_k)$ are a set of free-fermion eigenstates with momentum m_k . Thus, the fermionized quasi particles form a shifted Fermi sea. Here, $\hat{b}_{x_i}^\dagger$ is the creation operator of the i -th boson obeying to the relation $[\hat{b}_{x_i}, \hat{b}_{x'_i}^\dagger] = 0$ for $x_i \neq x'_i$. The on-site constraints are $\hat{b}_{x_i}^\dagger \hat{b}_{x_i}^\dagger = \hat{b}_{x_i} \hat{b}_{x_i} = 0$ and $\{\hat{b}_{x_i}, \hat{b}_{x_i}^\dagger\} = 1$. Substituting Eq. (S21) into Eq. (S15), we have

$$W_{II'} = \int dx^N \tan \left[\sum_i^N K \cos(x_i) / 2\hbar_{\text{eff}} \right] \mathcal{A} \det [\psi_{m_k}^I(x_k)]^* \mathcal{A} \det [\psi_{m_k}^{I'}(x_k)], \quad V_I = \tan \left[\left(\sum_{k=1}^N \frac{\hbar_{\text{eff}}^2 m_k^2}{2} - \theta_\alpha \right) \frac{T}{2\hbar_{\text{eff}}} \right]. \quad (\text{S22})$$

When $\mathcal{A}^2 = 1$, the off-diagonal hopping reduces to the hopping of free fermions (FF), denoted by $W_{II'}^{\text{FF}}$.

D. The center-of-mass coordinate frame

It is noteworthy that the LL Hamiltonian \hat{H}_I commutes with the total momentum operator \hat{P}

$$[\hat{H}_I, \hat{P}] = 0, \quad \hat{P} = \sum_i^N \hat{p}_i. \quad (\text{S23})$$

Thus the LL eigenstates can be factorized as two parts:

$$|I\rangle = |\psi_Q\rangle \otimes |\psi_{q_1, q_2, \dots}\rangle \quad (\text{S24})$$

where $|\psi_Q\rangle$ is a plane wave with the total momentum Q , the rest wave function $|\psi_{q_1, q_2, \dots}\rangle$ is about the relative momenta q_1, q_2, \dots . The off-diagonal term $W_{II'}$ can be simplified as follows:

$$\begin{aligned} W_{II'} &= \langle I | \tan(\hat{H}_K/2\hbar_{\text{eff}}) | I' \rangle \\ &= \langle \psi_{q_1, q_2, \dots} | \langle \psi_Q | \tan(\hat{H}_K/2\hbar_{\text{eff}}) | \psi_{Q'} \rangle | \psi_{q'_1, q'_2, \dots} \rangle \\ &= \int dx_{r_1} dx_{r_2} \cdots dx_{r_N} \psi_{q_1, q_2, \dots} \psi_{q'_1, q'_2, \dots}^* \int dx_c \tan \left[\sum_i^N K \cos(x_i)/2\hbar_{\text{eff}} \right] e^{-i(Q-Q')x_c} \end{aligned} \quad (\text{S25})$$

where x_c, x_r, x_i denote the center-of-mass, relative and total coordinate. Noticing the identity that

$$\begin{aligned} \sum_i^N \cos(x_i) &= \sum_i^N \cos(x_c + x_{r_i}/N) \\ &= \cos(x_c) \sum_i^N \cos(x_{r_i}/N) - \sin(x_c) \sum_i^N \sin(x_{r_i}/N) \\ &= \frac{1}{\sqrt{[\sum_i^N \cos(x_{r_i}/N)]^2 + [\sum_i^N \sin(x_{r_i}/N)]^2}} \cos[x_c + \phi(x_{r_1}, x_{r_2}, \dots)], \end{aligned} \quad (\text{S26})$$

where we introduce a phase factor $\phi(x_{r_1}, x_{r_2}, \dots)$ about the relative coordinate

$$\cos[\phi(x_{r_1}, x_{r_2}, \dots)] = \frac{\sum_i^N \cos(x_{r_i}/N)}{\sqrt{[\sum_i^N \cos(x_{r_i}/N)]^2 + [\sum_i^N \sin(x_{r_i}/N)]^2}}. \quad (\text{S27})$$

Thus, we have

$$W_{II'} = \int dx_{r_1} dx_{r_2} \cdots dx_{r_N} \psi_{q_1, q_2, \dots} \psi_{q'_1, q'_2, \dots}^* W_{QQ'}(x_{r_1}, x_{r_2}, \dots) \quad (\text{S28})$$

with

$$W_{QQ'}(x_{r_1}, x_{r_2}, \dots) = \int dx_c \tan \{ K \cos[x_c + \phi(x_{r_1}, x_{r_2}, \dots)]/2\hbar_{\text{eff}} \} e^{-i(Q-Q')x_c}. \quad (\text{S29})$$

If we fix all the relative coordinate x_{r_1}, x_{r_2}, \dots , the phase factor $\phi(x_{r_1}, x_{r_2}, \dots)$ is a constant. Then $W_{QQ'}$ has the same form as that of the single-particle QKR, which is known to decay exponentially fast. Therefore, generally for any number of particles, we expect DL always holds in the center-of-mass momentum.

S4. TWO-PARTICLE CASE IN THE LATTICE MAPPING

We consider two bosons, with positions (x_1, x_2) and treat them in a center of mass and relative coordinates frame ($x_c = (x_1 + x_2)/2$, $x_r = x_1 - x_2$). Then, the eigenfunction of the Lieb-Liniger model \hat{H}_I reads [23]

$$\psi_Q^q(x_c, x_r) = \begin{cases} \sqrt{\frac{1}{\pi}} B_Q^q \cos[qx_r - (q + Q)\pi] e^{2iQx_c}, & \text{if } 0 \leq x_r \leq 2\pi, \\ \sqrt{\frac{1}{\pi}} B_Q^q \cos[qx_r + (q + Q)\pi] e^{2iQx_c}, & \text{if } -2\pi \leq x_r \leq 0, \end{cases} \quad (\text{S30})$$

where $B_Q^q = [8\pi + (4/q) \sin(2q\pi) \cos(2Q\pi)]^{-1/2}$ and $2(q + Q)\pi = \pi - 2 \arctan(2qA_g)$ with an inverse interaction strength $A_g = \hbar_{\text{eff}}^2/g$. Q is the center-of-mass momentum with $Q = 0, \pm 1/2, \pm 1, \pm 3/2, \dots$, and q is the relative momentum. Thus, the eigenenergy is given by $E_Q^q = \hbar_{\text{eff}}^2(Q^2 + q^2)$.

Having obtained the eigenfunction, the off-diagonal term $W_{QR}^{qq'}$ in the lattice mapping is given by

$$W_{QQ'}^{qq'} = 2 \iint \psi_Q^q(x_c, x_r) \tan \left[\frac{K}{\hbar_{\text{eff}}} \cos x_c \cos \frac{x_r}{2} \right] \psi_{Q'}^{q'}(x_c, x_r)^* dx_c dx_r. \quad (\text{S31})$$

Then, utilizing the periodicity of function, we have a simpler expression as

$$W_{QQ'}^{qq'} = \frac{1}{\pi} B_Q^q B_{Q'}^{q'} \int_0^{2\pi} \left\{ \cos[\phi_+(x_r)] + \cos[\phi_-(x_r)] \right\} \mathcal{B}_{Q-Q'}(x_r) dx_r, \quad (\text{S32})$$

where

$$\begin{aligned} \mathcal{B}_{Q-Q'}(x_r) &= 2 \int_0^{2\pi} \tan \left[\frac{K}{\hbar_{\text{eff}}} \cos x_c \cos \frac{x_r}{2} \right] e^{2i(Q-Q')x_c} dx_c, \\ \phi_{\pm}(x_r) &= (q \pm q')x_r - (q \pm q' + Q \pm Q')\pi. \end{aligned} \quad (\text{S33})$$

After calculating a series of integrals, we have

$$W_{QQ'}^{qq'} = \frac{1}{\pi} B_Q^q B_{Q'}^{q'} \sum_{s=\pm} \left[C_1^s + C_2^s + C_3^s + \cdots + C_n^s + \mathcal{D}_n^s \right], \quad (\text{S34})$$

where

$$\begin{aligned} C_{2i-1}^{\pm} &= \frac{(-1)^{i+1} \mathcal{B}_{Q-Q'}^{(2i-2)}(x_r) \sin[\phi_{\pm}(x_r)]}{(q \pm q')^{2i-1}} \Big|_0^{2\pi}, & C_{2i}^{\pm} &= \frac{(-1)^{i+1} \mathcal{B}_{Q-Q'}^{(2i-1)}(x_r) \cos[\phi_{\pm}(x_r)]}{(q \pm q')^{2i}} \Big|_0^{2\pi}, \\ \mathcal{D}_{2i-1}^{\pm} &= \frac{(-1)^i \int_0^{2\pi} \mathcal{B}_{Q-Q'}^{(2i-1)}(x_r) \sin[\phi_{\pm}(x_r)] dx_r}{(q \pm q')^{2i-1}}, & \mathcal{D}_{2i}^{\pm} &= \frac{(-1)^i \int_0^{2\pi} \mathcal{B}_{Q-Q'}^{(2i)}(x_r) \cos[\phi_{\pm}(x_r)] dx_r}{(q \pm q')^{2i}}, \end{aligned} \quad (\text{S35})$$

with $\mathcal{B}_{Q-Q'}^{(n)} = d^n \mathcal{B}_{Q-Q'}(x_r) / dx_r^n$. Since $\mathcal{B}_{Q-Q'}(x_r)$ is an even function with a period of 4π , we have $\mathcal{B}_{Q-Q'}^{(2i-1)}(0) = \mathcal{B}_{Q-Q'}^{(2i-1)}(2\pi) = 0$, implying $C_{2i}^{\pm} = 0$. Then, considering the leading order $C_1^{\pm} + C_3^{\pm}$ and $\mathcal{B}_{Q-Q'}(2\pi) = -\mathcal{B}_{Q-Q'}(0)$, $\mathcal{B}_{Q-Q'}^{(2)}(2\pi) = -\mathcal{B}_{Q-Q'}^{(2)}(0)$, we have

$$\begin{aligned} C_1^+ + C_1^- &= 2\mathcal{B}_{Q-Q'}(0) \frac{\sin[(Q+Q')\pi] \cos[(q+q')\pi]}{q+q'} + 2\mathcal{B}_{Q-Q'}(0) \frac{\sin[(Q-Q')\pi] \cos[(q-q')\pi]}{q-q'}, \\ C_3^+ + C_3^- &= -2\mathcal{B}_{Q-Q'}^{(2)}(0) \frac{\sin[(Q+Q')\pi] \cos[(q+q')\pi]}{(q+q')^3} - 2\mathcal{B}_{Q-Q'}^{(2)}(0) \frac{\sin[(Q-Q')\pi] \cos[(q-q')\pi]}{(q-q')^3}. \end{aligned} \quad (\text{S36})$$

We note that if Q and Q' are integers or half-integers, the above equations equal to 0.

Next, considering that Q is a half-integer, Q' is an integer, and $\sin[(Q+Q')\pi] = 1$, we have

$$C_1^+ + C_1^- = 2\mathcal{B}_{Q-Q'}(0) \frac{2q \cos(q\pi) \cos(q'\pi) + 2q' \sin(q\pi) \sin(q'\pi)}{q^2 - q'^2}, \quad (\text{S37})$$

where

$$\mathcal{B}_{Q-Q'}(0) = 2 \int_0^{2\pi} \tan \left[\frac{K}{\hbar_{\text{eff}}} \cos x_c \right] e^{2i(Q-Q')x_c} dx_c. \quad (\text{S38})$$

Using $2(q+Q)\pi = \pi - 2 \arctan(2qA_g)$, $2q/\tan(q\pi) = -1/A_g$, and $2q'\tan(q'\pi) = 1/A_g$, we have

$$C_1^+ + C_1^- = 0. \quad (\text{S39})$$

Considering $q \gg q'$, we also have

$$C_3^+ + C_3^- = -2\mathcal{B}_{Q-Q'}^{(2)}(0) \frac{2 \cos(q\pi) \cos(q'\pi)}{q^3}. \quad (\text{S40})$$

Then, since

$$\cos(q\pi) = \frac{\pm 1}{\sqrt{[1 + (2qA_g)^2]}}, \quad \cos(q'\pi) = \frac{\pm 2q'A_g}{\sqrt{[1 + (2q'A_g)^2]}}, \quad (\text{S41})$$

we have

$$C_3^+ + C_3^- = -4\mathcal{B}_{Q-Q'}^{(2)}(0) \frac{\pm 1}{\sqrt{[1 + (2qA_g)^2]}} \frac{\pm 2q'A_g}{\sqrt{[1 + (2q'A_g)^2]}} \frac{1}{q^3}. \quad (\text{S42})$$

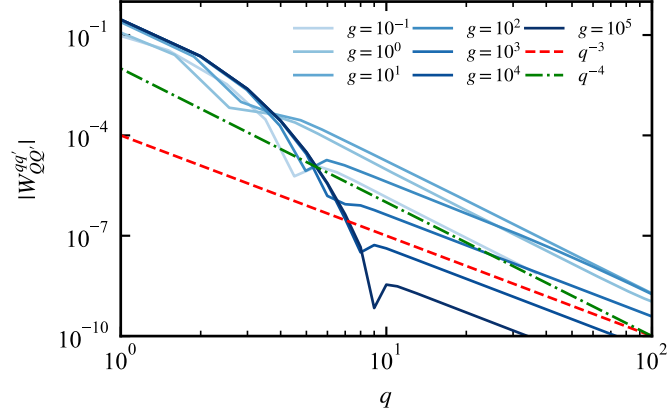


Figure S1. The off-diagonal term $|W_{QQ'}^{qq'}|$ from Eq. (S31) as a function of relative momentum q for different interaction strengths. The red and green dashed lines denote algebraic decay as q^{-3} and q^{-4} , respectively. The kick strength is $K = 1$ and here we set $Q' = 0$, $Q = 0.5$.

Considering large q , B_Q^q and $B_{Q'}^{q'} \sim [\sqrt{8\pi}]^{-1}$, we arrive at

$$|W_{QQ'}^{qq'}| \sim \left| \frac{\mathcal{B}_{Q-Q'}^{(2)}(0)}{2\pi^2} \frac{1}{\sqrt{[1 + (2qA_g)^2]}} \frac{2q'A_g}{\sqrt{[1 + (2q'A_g)^2]}} \frac{1}{q^3} \right|, \quad (\text{S43})$$

where

$$\mathcal{B}_{Q-Q'}^{(2)}(0) = \int_0^{2\pi} \frac{K \cos x_c}{2\hbar_{\text{eff}} \cos^2 \left[\frac{K}{\hbar_{\text{eff}}} \cos x_c \right]} e^{2i(Q-Q')x_c} dx_c, \quad (\text{S44})$$

decays exponentially fast with $Q - Q'$. Especially, we consider fixed q' and finite q . For weak interaction ($A_g \rightarrow \infty$), $2qA_g \gg 1$, $2q'A_g \gg 1$ one finds that

$$|W_{QQ'}^{qq'}| \sim \left| \frac{\mathcal{B}_{Q-Q'}^{(2)}(0)}{4\pi^2 A_g} \frac{1}{q^4} \right|, \quad (\text{S45})$$

whereas for the TG limit ($A_g \rightarrow 0$), we have $2qA_g \ll 1$, $2q'A_g \ll 1$, and

$$|W_{QQ'}^{qq'}| \sim \left| \frac{\mathcal{B}_{Q-Q'}^{(2)}(0)q'A_g}{\pi^2} \frac{1}{q^3} \right|. \quad (\text{S46})$$

For integer Q and half-integer Q' , one can arrive at the same result. Therefore, from the viewpoint of the lattice mapping, the tails of off-diagonal hopping for weak and strong interactions exhibit distinct decay behaviors. Notably, the amplitude of the tail at weak interaction contributes a lot ($\propto A_g^{-1}$), whereas it becomes smaller and even negligible with the increase of interactions ($\propto A_g$). This explains the absence of tail in Eq. (S22). As shown in Fig. S1, as g increases, the amplitude of tail undergoes a nonmonotonic change and the exponent changes from q^{-4} to q^{-3} .

S5. ADDITIONAL RESULTS OF THE OFF-DIAGONAL TERM IN THE LATTICE MAPPING

Here we show more details about the tail's crossover of the off-diagonal term $|W_{II'}|$ with increasing interactions. As shown in Fig. S2 (a1-a5), when $g \leq 10$, i.e. in regime I, the off-diagonal term always exhibits a tail as E_I^{-2} , whereas the amplitude of the tail increases with increasing g . As g increases into regime II, the tail dramatically changes, approaching $E_I^{-3/2}$ and its amplitude becomes smaller. This nonmonotonic change aligns with the two-particle prediction. If we start from an initial excited state, the crossover behavior of the tail is same, as shown as curves of $|W_{4I}|$ (b1-b5) and $|W_{8I}|$ (c1-c5) in Fig. S2.

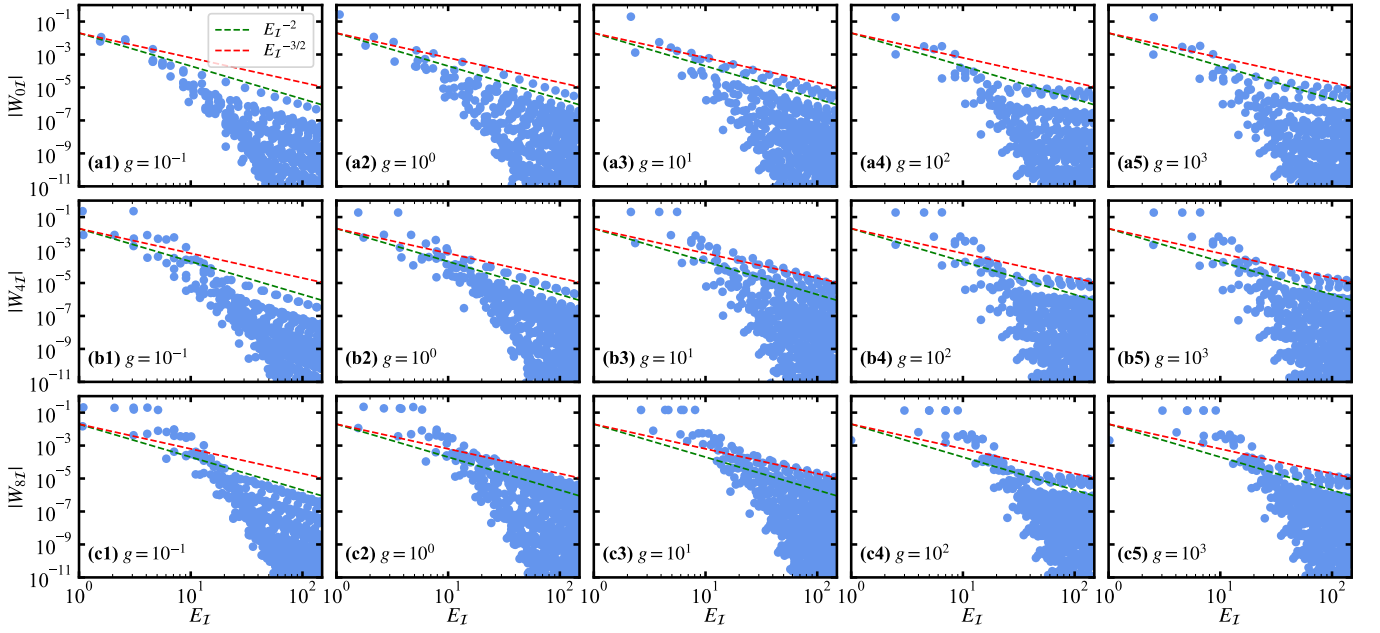


Figure S2. (a1-a5) The off-diagonal term $|W_{0I}|$ as a function of energy E_I for different interactions. The red and green dashed lines denote algebraic decay as $E_I^{-3/2}$ and E_I^{-2} , respectively. The cut-off, the kick strength and the particle number are $M = 35$, $K = 0.5$ and $N = 3$, respectively. (b1-b5) The same data as in (a1-a5) but for $|W_{4I}|$. (c1-c5) The same data as in (a1-a5) but for $|W_{8I}|$.

S6. OCCUPATION SPECTRUM OF THE ONE-PARTICLE DENSITY MATRIX

We can also characterize the deep MBDL regime (small K) using the one-particle density matrix (OPDM). In the Fock basis, given a Floquet eigenstate $|\psi\rangle$, the OPDM is defined as [55, 61]

$$\rho_{mn} = \langle \psi | \hat{b}_m^\dagger \hat{b}_n | \psi \rangle. \quad (\text{S47})$$

The natural orbitals (NOs) $|\phi_\alpha\rangle$ and occupations n_α are obtained by diagonalizing ρ

$$\rho |\phi_\alpha\rangle = n_\alpha |\phi_\alpha\rangle. \quad (\text{S48})$$

For interaction-free scenario, the NOs are the single-particle Anderson orbitals. In the presence of interactions, we can consider the NOs as the quasi-particle orbitals. The total occupations are $\sum_\alpha n_\alpha = N$, and n_α is similar to the quasi-local integrals of motion in the effective Hamiltonian for the MBL phase [61, 62].

We show the averaged \bar{n}_α for different g ranging from $g = 0.1$ to $g = 100$ in Fig. S3. For $N = 3$ and $g \leq 10$, we find that \bar{n}_α mainly distribute at the first N orbitals where $\bar{n}_\alpha \approx 1$ (see in the inset of Fig. S3(a)). This is a strong localization similar to the single-particle scenario. When the system leaves regime (I) ($g = 100$), the largest \bar{n}_α almost halves with a wider distribution, which still present localization. This corresponds to the extend property of the Floquet eigenstates. Remarkably different from the single-particle scenario, \bar{n}_α exhibit an algebraic tail, asymptotically falling as α^{-4} for $g \leq 10$ while α^{-2} at $g = 100$. The crossover between two algebraic tails is much pronounced in the scenario of $N = 2$ due to larger cut-off M (Fig. S3(b)). These tails are induced by long-range hoppings $\hat{H}_{\text{IOD}} = \frac{g}{2L} \sum_{m \neq p, m \neq q} \hat{b}_m^\dagger \hat{b}_n^\dagger \hat{b}_p \hat{b}_q \delta_{m+n, p+q}$ and show the coherence of the interacting bosons in Fock basis. Such a crossover also corresponds to the jump behavior of D_β and b_β as the interaction strength g increases.

S7. ADDITIONAL RESULTS OF THE HOPPING AMPLITUDE IN FOCK BASIS

In the main text, we show a specific case that the hopping amplitude from the BEC state $|0, 0\rangle$, whose kinetic energy is zero. In this section, we also consider initial states as highly excited ones $|p_c \neq 0, \Delta p = 0\rangle$ and $|p_c = 0, \Delta p \neq 0\rangle$. Figure S4 shows the hopping amplitude of standard deviation spreading (a1-a5) $|U_{p_c p_c}^{\Delta p 0}|$ and center-of-mass momentum expansion $|U_{p_c 0}^{\Delta p \Delta p}|$ (b1-b5) for different interaction strengths. We find that for various initial momenta, the decay behaviors remain almost identical. With increasing interaction strength, all algebraic tails in $|U_{p_c p_c}^{\Delta p 0}|$ consistently change from Δp^{-2} to Δp^{-1} . The amplitudes of center-of-mass momentum expansion $|U_{p_c 0}^{\Delta p \Delta p}|$ follow the same fast decay. The localization length is almost independent of interactions and initial standard deviation Δp .

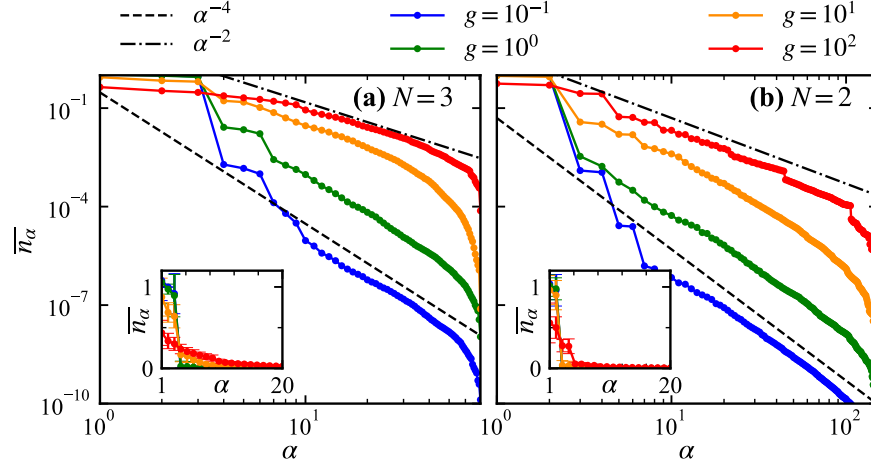


Figure S3. (a) The occupation spectrum \bar{n}_α for the particle number $N = 3$ and different interaction strength g . The inset shows the same data but in linear scale. The cut-off and the kick strength are $M = 30$ and $K = 0.1$. (b) The same data as in (a) but for $N = 2$ and $M = 75$. The results are obtained by average over 50 Floquet eigenstates.

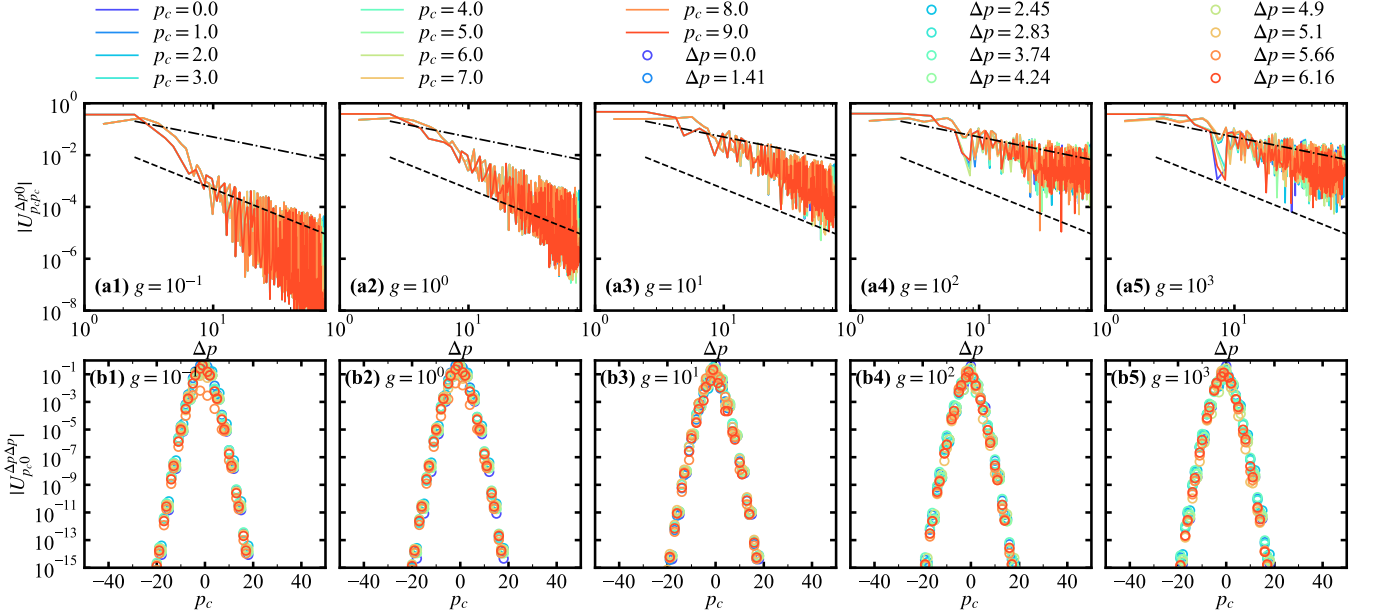


Figure S4. (a1-a5) The hopping amplitude $|U_{p_c p_c}^{\Delta p 0}|$ as a function of the standard deviation Δp for different interactions g in log-log scale. The dashed line and dot-dashed line denote algebraic decay as Δp^{-2} and Δp^{-1} , respectively. (b1-b5) The hopping amplitude $|U_{p_c 0}^{\Delta p \Delta p}|$ as a function of the center-of-mass momentum p_c for different interactions g in a semi-log scale. The particle number, cut-off and kick strength are $N = 3$, $M = 30$ and $K = 1$, respectively.

S8. KICKING A NONEQUILIBRIUM STATE AT DIFFERENT INTERACTIONS

Usually, the MBDL is achieved by kicking a low-energy state, i.e. near ground state of the Lieb-Liniger Hamiltonian. Here, in Fock basis, we consider a nonequilibrium state, i.e., the Fock state $|\alpha\rangle \equiv |p_c, \Delta p\rangle$. Since \hat{U} decays algebraically on the standard deviation, the momentum distribution $n(m) = \langle \hat{b}_m^\dagger \hat{b}_m \rangle$ is expected to own a long tail at large momentum. For experimental feasibility, we start from the zero-momentum state $|0, 0\rangle$, where all bosons condensate at zero momentum. Figure S5 shows the momentum evolution for different interaction and particle numbers at $K = 1$. After 100 kicks, we find that the kinetic energy E_m saturates and the momentum distribution $n(m)$ stops spreading. As expected, $n(m)$ exhibits an algebraic decay as $n(m) \propto m^{-\eta}$ at large momentum regime, while it nearly exponentially decays at low momentum. At regime I ($g = 1$), the decaying exponent

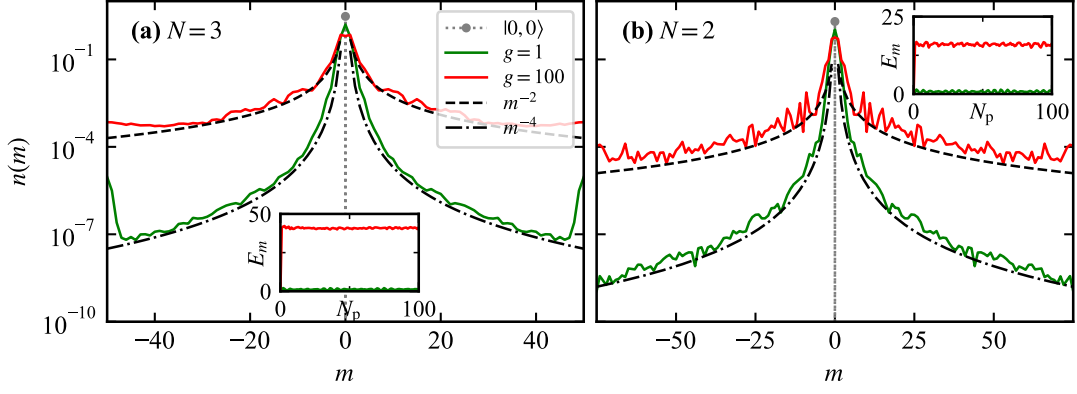


Figure S5. (a) The momentum distribution $n(m)$ after 100 kicks for different interaction strength g . The cut-off, kick strength and particle number are $M = 50$, $K = 1$ and $N = 3$, respectively. The gray dashed line denotes the initial zero-momentum state. The inset shows the corresponding kinetic energy evolution. (b) The same data as in (a) but for $N = 2$ and $M = 75$. N_p denotes the kick number.

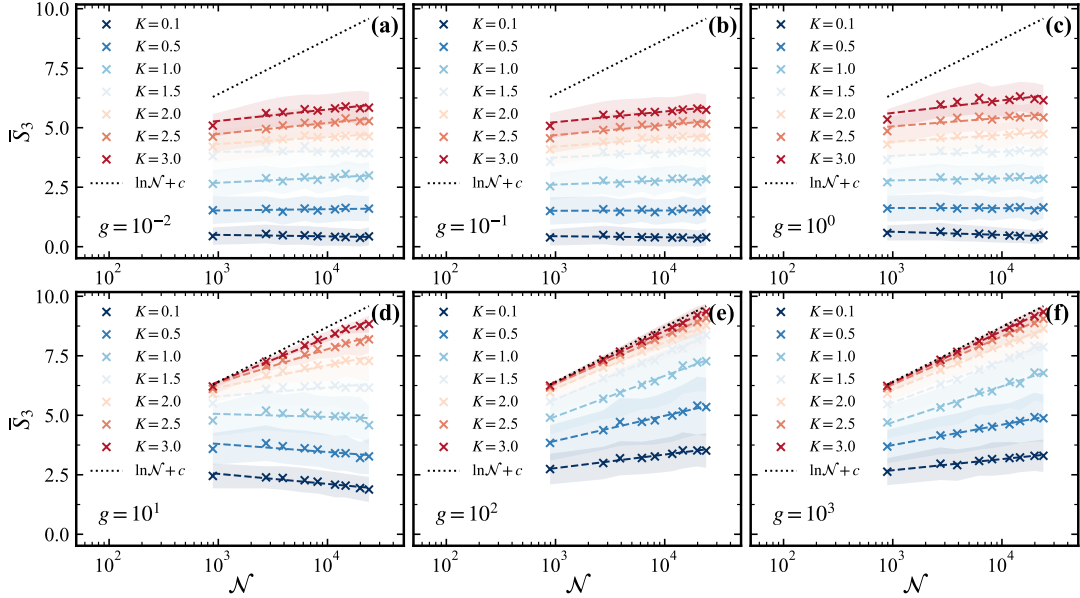


Figure S6. The linear fittings (dashed lines) of \bar{S}_3 as a function of dimension \mathcal{N} for different g and K . The shaded areas denote the standard deviation obtained by the average over 500 eigenstates. The number of bosons is fixed as $N = 3$.

is $\eta = 4$. This exhibits the same signature of the MBDL by kicking the ground state of interacting bosons. Strikingly, it is distinct that η turns into 2 at $g = 100$, similar to the occupation spectrum. It has been studied that the momentum distribution from quenching a zero-momentum state in the pristine Lieb-Liniger model presents different tails for different interactions. The tail m^{-2} is the manifestation of fermionic excitation. We find that periodic kicks do not destroy this signature. Since the zero-momentum state has nearly the same energy as the Lieb-Liniger ground state at small g , it is not surprising that $n(m) \propto m^{-4}$. Yet the interacting energy $\langle 0, 0 | \hat{H}_1 | 0, 0 \rangle$ is significantly large at $g \rightarrow \infty$, which is far from equilibrium. In this sense, MBDL is also present even if we kick a nonequilibrium state with high initial energy.

S9. THE FITTING PROCEDURE OF THE GENERALIZED FRACTAL DIMENSION

To identify the possible dominant asymptotic behaviors of the PE S_β as the dimension \mathcal{N} grows, we utilize a scaling form $\bar{S}_\beta = D_\beta \ln \mathcal{N} + b_\beta$. In particular, the PE at $\beta = 1$ is the Shannon entropy $S_1 = -\sum_\alpha |\psi_\alpha|^2 \ln |\psi_\alpha|^2$ while $\beta = 2$ gives the inverse participation ratio (IPR) with $S_2 = -\ln(\text{IPR})$. Note that, a larger kick strength induces a longer localization length l_{loc} in the truncated momentum space M . One needs to push the cutoff towards infinity so that $M \gg l_{\text{loc}}$ to guarantee the convergence,

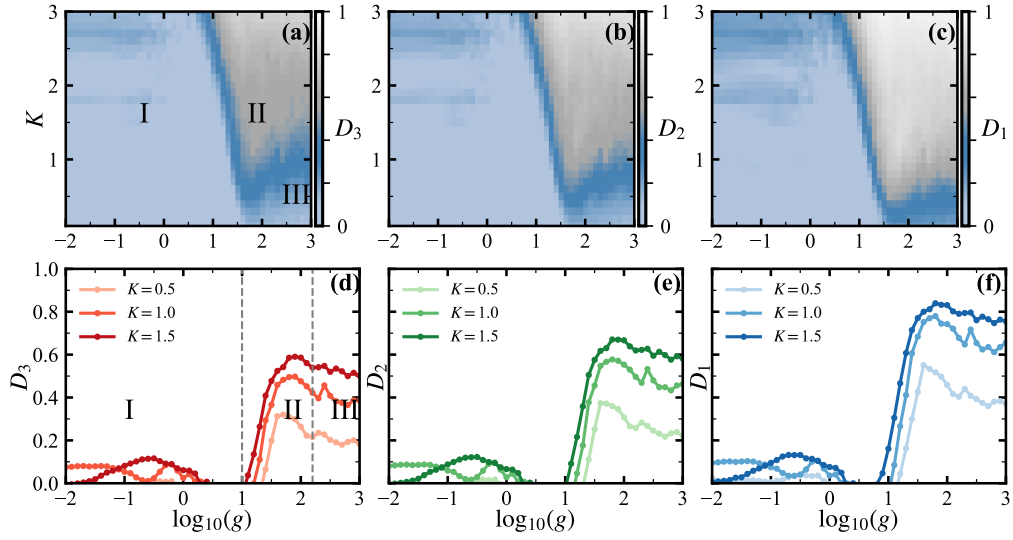


Figure S7. The fractal dimensions (a) D_3 , (b) D_2 , and (c) D_1 as a function of the interaction strength g and the kick strength K , respectively. The number of bosons is $N = 3$. The area at large K represent numerical inaccurate regime due to finite truncation. (d-f) Different D_β as a function of g at different K . The gray dashed lines denote the regime boundaries.

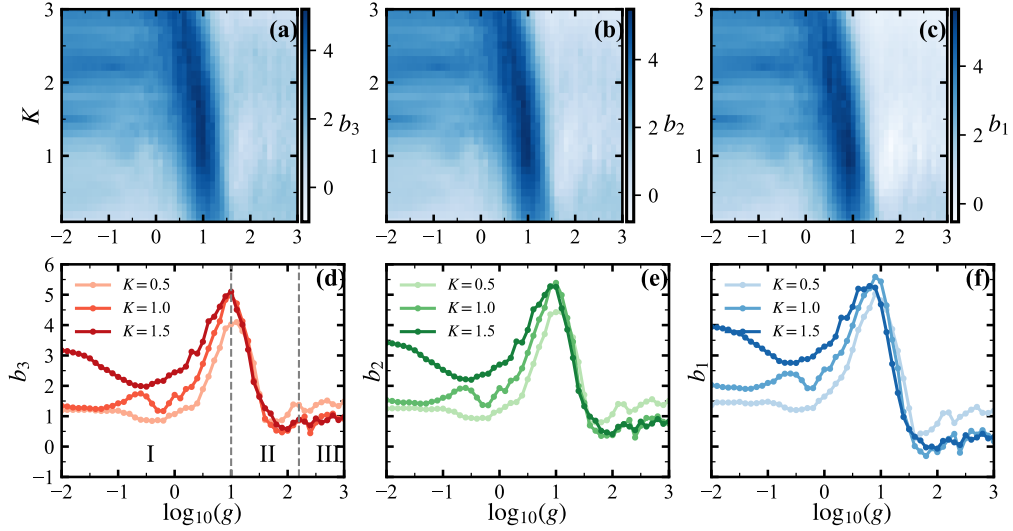


Figure S8. The fitted intercepts (a) b_3 , (b) b_2 , and (c) b_1 as a function of the interaction strength g and the kick strength K , respectively. The number of bosons is $N = 3$. (d-f) Different b_β as a function of g for different K . The gray dashed lines denote the regime boundaries.

which is quite challenging in ED simulations. This restricts the range of kick and interaction strengths considered, as the condition $g \gtrsim LM^2$ is unphysical for finite g .

Figure S6 shows the fitting details of S_3 for various interaction strengths and kick strengths. The linear fitting seemingly works very well and the standard deviations are controllable in a small range. The linear fittings of other PE (S_2, S_1) are similar. Intuitively, the dimension is always positive, whereas for small K and $g = 10^1$ we find anomaly that $D_3, D_2, D_1 < 0$. This might be attributed to the closeness to the crossover between regimes I and II. Through this approach, we extract the fitted slopes as the fractal dimensions D_β , then obtain their 2D diagram as a function of g and K , as shown in Fig. S7(a-c). One can see that different D_β gives a roughly similar behavior, in the sense that there are always three regimes separated by different values. Regime II is remarkable in D_1 diagram. If the kick strength K is fixed, we can find the non-monotonic behavior with the increase of g as shown in Fig. S7(d-f). As g increases, all $D_{\beta=1,2,3}$ jump to a peak value followed by a decrease. For weak interaction regime, say $g \sim 10^{-1}$, the system is close to free bosons, whereas after the peak regime (regime III) the system is fermionization and thus it can be described by free fermions. This implies the origin of the non-monotonic behavior.

Furthermore, another quantity is the fitted intercept b_β . In the context of many-body localization, the sign of b_β signifies the

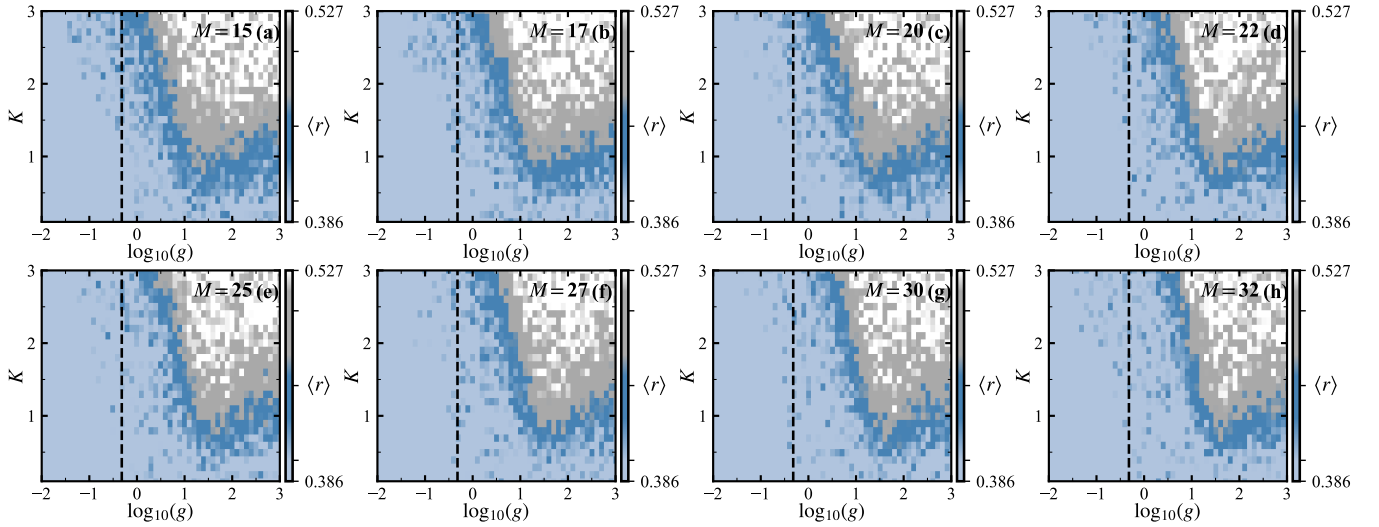


Figure S9. The averaged energy spacing ratio $\langle r \rangle$ as a function of the interaction strength g and the kick strength K for different cut-off M . The number of bosons is $N = 3$. The area at large K represents numerical inaccurate regime due to finite truncation.

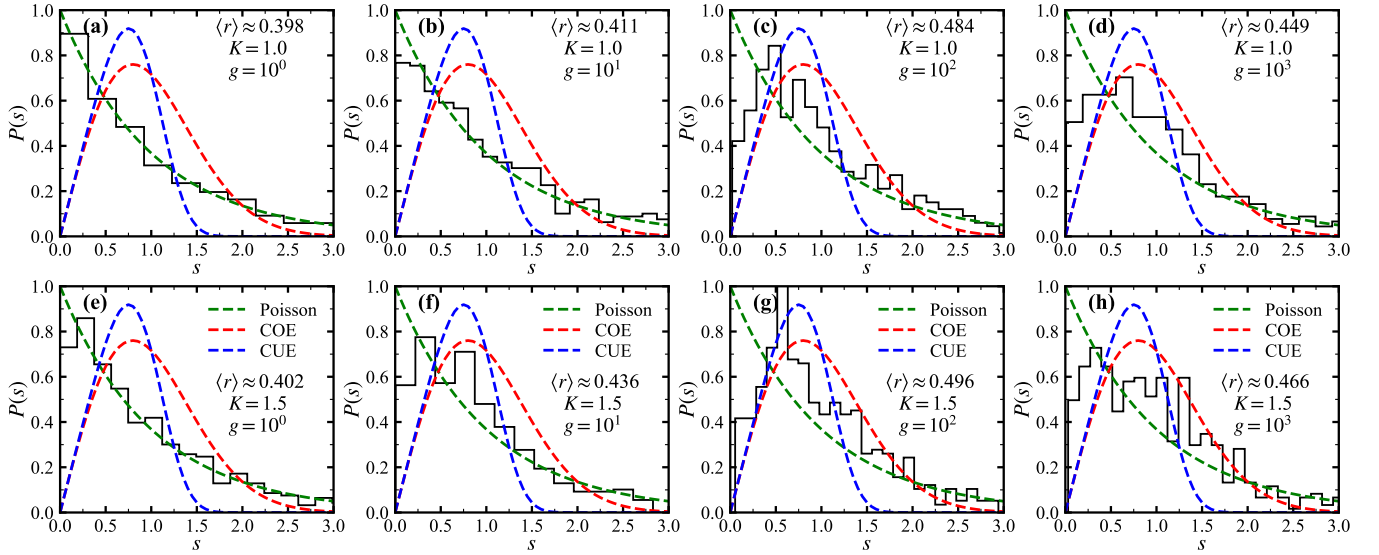


Figure S10. The histograms of the level-spacing distributions $P(s)$ for different kick strength and interactions. The number of bosons and cut-off is $N = 3$ and $M = 32$, respectively. The green dashed line, the red dashed line and the purple dashed lines denote the Poisson, the COE and the CUE distribution.

boundary between localization and ergodicity [52]. Figure S8(a-c) also shows the fitted intercept b_β as a function of g and K . Interestingly, b_β exhibits similar crossovers between three regimes as D_β . One can also find the non-monotonic behavior in Figs. S8(d-f), but it is different that b_β suddenly drops when D_β increases. The non-monotonic behavior of D_β and b_β signifies different characterizations of the MBDL phase. Notably, $b_\beta > 0$ almost always holds for small K , whereas $b_\beta < 0$ happens for large K and g . As we discussed before, the numerical accuracy for large K are limited by the cut-off. At least, there is no ergodicity in the low K regime, say $K < 3$. Nevertheless, b_β is approaching to 0 at regime II, signifying the scalability nature of the system.

S10. THE ENERGY LEVEL-SPACING STATISTICS

Considering the finite cut-off M in momentum space, here we study its effect on the level-spacing statistics in Fig. S9. Despite some differences at small g and large K , all the $\langle r \rangle$ diagrams exhibit a similar behavior. Note that the weak-interacting bosons are

in strong degeneracy, which is solved after $\gamma = 1$ (the dashed line). Even for the smallest M , there exists a cone (V-shape pattern in $\langle r \rangle$ diagrams) at the TG regime. As M increases, the cone at regime II becomes clearer. Therefore, our results are reasonable even under the finite cut-off and the cone regime is expected to persist as the cut-off is pushed toward infinity. For the largest M , we further pick two different kick strengths to see the details by the level-spacing distribution, which contains more information than $\langle r \rangle$. With the consecutive energy gaps $\delta_\alpha = \theta_{\alpha+1} - \theta_\alpha$, we count the frequency with which the energy gap occurs in a certain range and plot the histogram. Figure S10 shows the level-spacing distributions $P(s)$ for different K and g , where $s = \delta_\alpha / \langle \delta_\alpha \rangle$. For an integrable system, $P(s)$ follows the Poisson distribution (green). For an ergodic Floquet system with time-reversal symmetry, $P(s)$ follows the circular orthogonal ensemble (COE) type, whereas with broken time-reversal symmetry it follows the circular unitary ensemble (CUE) type [56]. According to the random matrix theory, the exact formulas for the above three distributions are as follows [49]:

$$P_{\text{Poisson}}(s) = e^{-s}, \quad P_{\text{COE}}(s) = \frac{\pi}{2} s e^{-\pi s^2/4}, \quad P_{\text{CUE}}(s) = \frac{\pi}{2} s e^{-\pi s^4/4}. \quad (\text{S49})$$

When g is small at regime I, the level-spacing ratio suggest an integrable system. As shown in Fig. S10(a) and (e), $P(s)$ is well fitted by the Poisson distribution. As g increases, there are clear deviations appearing between $P(s)$ and the Poisson distribution and $P(s)$ show closeness to the COE distribution. However, such deviations become small with further increasing g . This non-monotonic behavior aligns with that of $\langle r \rangle$.